NTNU – Trondheim
Norwegian University of
Science and Technology

Dynamic Analysis of Fire Water Pump Module

Thomas Otto Størkson

Master of Science in Product Design and Manufacturing

Supervisor: Kjell H. Holthe, KT

Norwegian University of Science and Technology
Department of Structural Engineering

Institutt for konstruksjonsteknikk

Fakultet for ingeniørvitenskap og teknologi
NTNU – Norges teknisk-naturvitenskapelige universitet

MASTEROPPGAVE 2012

for

Thomas Otto Størkson

Title: *Dynamic Analysis of Fire Water Pump Module*

Background:
The noise requirements for offshore equipment are continuously getting stricter, and this thesis will be a contribution to the aim of reducing structure-born noise from the fire water pump module.

Problem:
The thesis will imply measurement of the dynamic response due to load generated by the system itself under normal operation, and further reviewing the results, in addition to validating the dynamic behavior using finite element analysis (Ansys). Finally, some simple researching will be attempted, searching for changes that can reduce the dynamic response, especially in the low frequencies.

Besvarelsen organiseres i henhold til gjeldende retningslinjer.

Hovedveileder:	Kjell Holthe	NTNU
Medveileder:	Sigve Gjerstad	FRAMO

Besvarelsen skal leveres til Institutt for konstruksjonsteknikk innen 11. juni 2012.

NTNU, 15. januar , 2012

Kjell Holthe

Kjell Holthe

Preface

I have been engaged in the Frank Mohn group since I first started there as an apprentice in 2003, and they have been giving me follow-up and aid since I started studying at NTNU in 2007. To write the master thesis for them and to better get to know their products from an engineering point of view is therefore a great pleasure before I am starting there as an employee in the technical department this summer 2012. I wish to thank both NTNU and the Frank Mohn group for good guidance throughout my studies.

My previous paper contained most of the presumed theory for the following thesis. The thesis contains a finite element analysis. Instead of using the software I was taught at NTNU, Abaqus, Frank Mohn Flatøy encouraged me to use the program they are using, Ansys. This required me to learn Ansys by attending a three day course arranged by EDR, in addition to doing a lot of tutorials by myself. I was also fortunate to spend some days at EDR's facilities in Sandvika to get guidance and verification regarding the model and analysis.
Special thanks to:

- my advisers, Prof. Kjell Holthe and Sigve Gjerstad for counselling and supervising.
- Ørjan Vatsøy, Tomas Laugsand Erlien and Jostein Smaamo at Frank Mohn Flatøy for help and advice along the way.
- Bjørn Tollefsen, Oddrun Myklebust and Frode Halvorsen at EDR Medeso for great coaching in Ansys
- Geir Hoseth from Scanditest for providing me with PulseShop student license from Brüel & Kjær.
- Danny P. Sleicher at RubberDesign BV for providing me with documentation on dampers.
- Børre Karlsrud at Centa Power Transmission for providing me with information about flexible couplings.
- my good friend, Zachary Livesay, and my beloved wife, Ingrid Gjesteland, for reading through my thesis, giving me feedback and checking my spelling and orthography.

Declaration

I declare that this paper was composed by myself, that the work contained herein is my own except where explicitly stated otherwise in the text, and that this work has not been submitted for any other degree or professional qualification except as specified.

Trondheim, 12th May 2012 Thomas Otto Størkson

Thomas Otto Størkson

Abstract

The thesis starts with a simple description of the system and some brief theory needed for the following analysis.

Further a factory acceptance test is performed, this implies measurement of the dynamic response due to load generated by the system itself under normal operation and making sure the dynamic behaviour are within the acceptance criteria. The data from the test is used to point out some weaknesses in the design from a dynamical point of view and some potential ideas of improvement are presented. To introduce additional damping of some of the rotational equipment is the idea which is proceeded with.

A great simplification in this thesis is that only transversal vibrations (the y-component of the vibrations) are considered after the factory acceptance test is performed. This results in less reliable quantities although the trends and the final conclusion remains correct.

A comprehensive finite element analysis is carried out to study the effect of a passive damper solution. It turns out that passive dampers can limit the vibrations remarkably, but if the foundation gets too soft the vibrations will increase. The low frequency vibration however, is not affected much by the additional damping. Some important eigenfrequencies are also studied and put into consideration. A sensitivity analysis of the constant damping ratio in the finite element solver is also performed.

In addition a more trivial analysis is performed to study the effect of an active damper solution. This solution seems to be less effective and does not influence the low frequencies considerably neither. It also introduces additional risk and weight to the system, which is highly undesirable.

The thesis concludes that passive damping of the hydraulic power unit has favourable effects on the system. If the main goal is to reduce low frequency vibration it might not be an entirely satisfying solution.

CONTENTS

LIST OF FIGURES

The cover picture in addition to figure 1.1, 1.2, 1.3, 1.4, 1.5 3.5(a), 3.5(b), 3.6, and 4.10 are provided by Frank Mohn Flatøy AS. Figure 1.6 and 1.7 are extracted from documentation provided by RubberDesign [12]. Figure 1.8(a) and 1.8(b) are extracted from documentation provided from Centa [5]. Figure 2.3 is extracted from tciauto.com. Figure 2.4 is extracted from popularmechanics.com. Figure 2.5 is extracted from atiracing.com. Figure 5.14(a) and 5.14(b) are extracted from Ho, Wong and England [18].

The remaining figures are self made.

LIST OF TABLES

NOMENCLATURE

AMD	Active Mass Damper
API	American Petroleum Institute
AVM	Anti Vibration Mount
CDR	Constant Damping Ratio
DE	Diesel Engine
FEM	Finite Element Method
FFT	Fast Fourier Transform
FRAMO	Frank Mohn
FRF	Frequency Response Function
FT	Fourier Transform
FWP	Fire Water Pump
H1	First harmonic: 29,2Hz
HPU	Hydraulic Power Unit
ISO	International Standard Organization
MR	Magneto-Rheological
PB	Booster Pump
RMS	Root Mean Square
SMD	Spring-Mass-Damper
TMD	Tuned Mass Damper

NOTATION

Latin letters

A_b	Bolt area	[m^2]
CDR	Constant damping ratio	[%]
c_k	Velocity amplitude	[$^m/_s$]
C_m	Cost coefficient	[$^{NOK}/_{kg}$]
D	Dynamic amplification	[-]
E	Youngs modulus	[Pa]
E_f/E_m,E_1/E_2	Youngs modulus of fibres/matrix and in 1/2-direction	[Pa]
f	Frequency	[Hz]
f_n	Eigenrequency	[Hz]
F	Load vector	[N]
k	Stiffness	[$^N/_m$]
$k_x/k_y/k_z$	Stiffness in x-/y-/z-direction	[$^N/_m$]
L	Length	[m]
m	Mass	[kg]
P	Load	[N]
P_k	Force amplitude	[N]
r	Response	[m]
R	Response vector	[$^m/_s$]
s	Side length	[m]
S	Auto spectrum	[$^{m^2}/_{(s^2 \cdot Hz)}$]
v_f	Volume fraction of fibre	[-]

Greek letters

β	Frequency ratio	[-]
ω	Frequency	[$^{rad}/_s$]
ω_n	Eigenfrequency	[$^{rad}/_s$]
ρ	Density	[$^{kg}/_{m^3}$]
ζ	Damping coefficient	[-]

Symbols with both latin and greek letters

ΔL	Deformation	[m]

1. INTRODUCTION

1.1 Problem description

The noise requirements for offshore equipment are continuously getting stricter and the Fire Water Pump Module is a loud mouthed machinery.

The system is tested every week and the excessive noise is annoying for the offshore workers. Some workers complained about the noise once, but after experiencing a fire they called back and apologized their complaint. They expressed that the roar of the module was music in their ears when the fire broke out.

The main aim of this thesis will be a contribution to the aim of reducing structure-born noise from the fire water pump module. Firstly, carrying out a concise factory acceptance test which is similar to the work I probably will be involved with next year. Secondly, using the collected data in addition to software and the best of my ability to propose potential ideas of design improvement.

Initially, a brief introduction of the system and some theory needed for the analysis and discussions are presented. Note that my last paper operated with $^{rad}/_{s}$ as angular velocity while this paper mainly operates with Hz, this is because I have noticed that Hz is the unit they use at FRAMO[1].

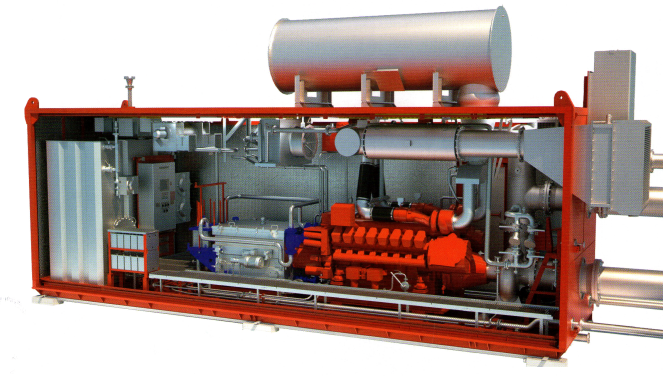

Fig. 1.1: The inventory of the fire water pump module

[1] Frank Mohn

1.2 Equipment description

The skid is the most interesting part from a dynamical point of view. The main sources of vibrations are the DE[2], the HPU[3] and PB[4]. This equipment in addition to the tank, is what is mounted on the skid; illustrated in figure 1.2. The container is also taken in to consideration in the FE model since it influences the stiffness and weight of the system greatly.

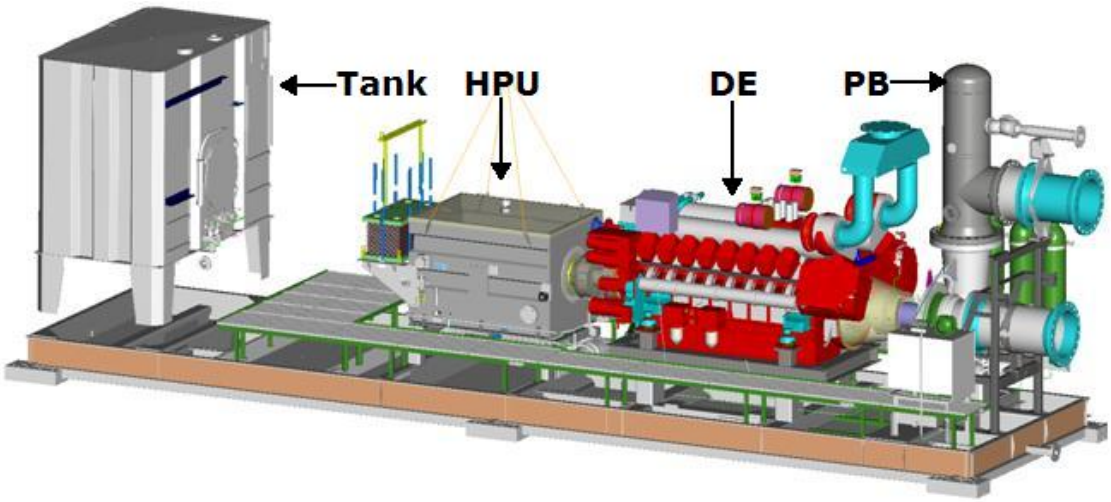

Fig. 1.2: Fire Water Pump System

1.3 Specifications

The module is $4250 \times 11300 \times 3100$mm, and it weighs 47000kg dry[5] and 61000kg wet[6]. The flow capacity of a system like this is typically 6200 m^3/h or 1722 l/s (for a physical interpretation, this flow is equivalent to six tank trucks of seawater per minute).

The significant equipment is all rotating with the same speed because both the HPU and the PB are directly driven by the engine, which runs at 1750rpm. Hence the load is dominated by harmonic loading with frequency equal to: $\frac{1750^{\text{rot}}/_{\text{min}}}{60^{\text{s}}/_{\text{min}}} \approx 29,2\text{Hz}$.

In addition loads will occur at multiples of this frequency, this is emphasized in section 2.2.

[2] Diesel Engine
[3] Hydraulic Power Unit
[4] Booster Pump
[5] Dry weight = Weight of the module alone
[6] Wet weight = Weight of the module + weight of the fluids in the system

Diesel engine

Manufracturer:	MTU
Power:	1808 kW
Weight (wet):	8190 kg (above dampers)
Rotational frequency:	29,2 Hz rpm

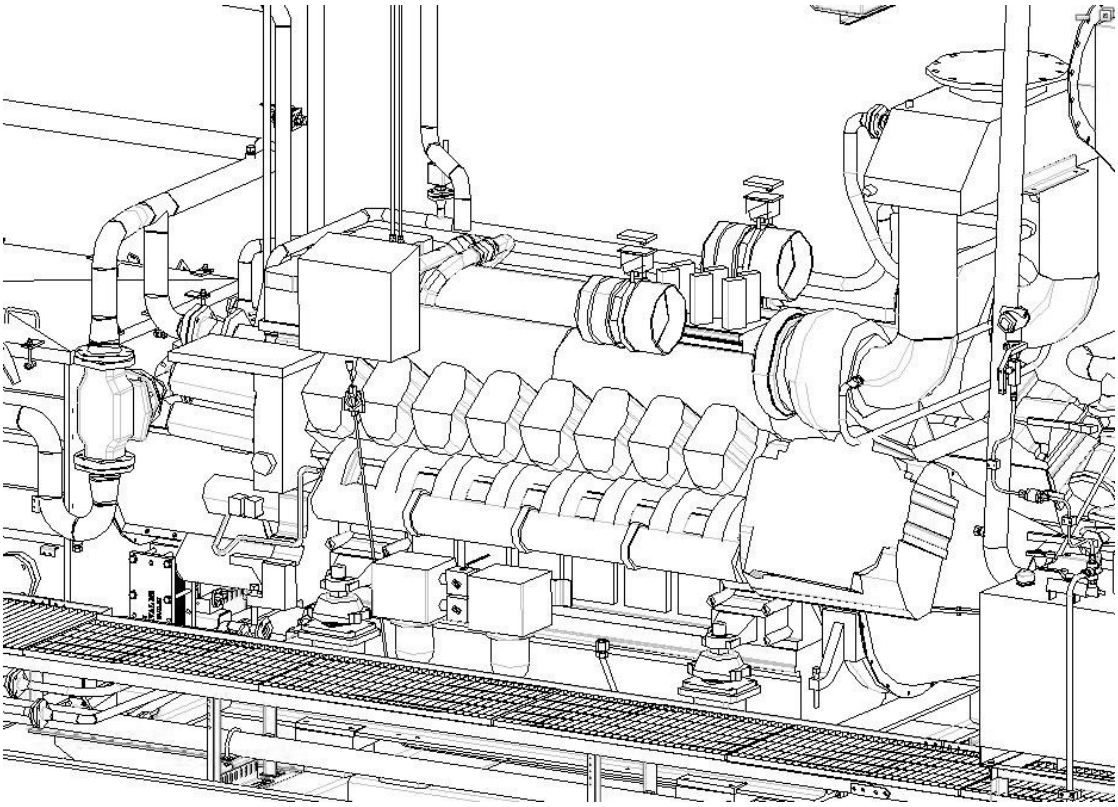

Fig. 1.3: 3D drawing of the diesel engine

The DE is V configured with 16 cylinders. It is also worth mentioning that the DE is mounted on passive dampers (AVM[7]). The specific AVMs are specified later in this section.

[7] Anti Vibration Mount

Hydraulic Power Pack

Manufracturer:	FRAMO
Power:	847 kW
Weight (wet):	(1800+500)=3300 kg
Rotational frequency:	29,2 Hz

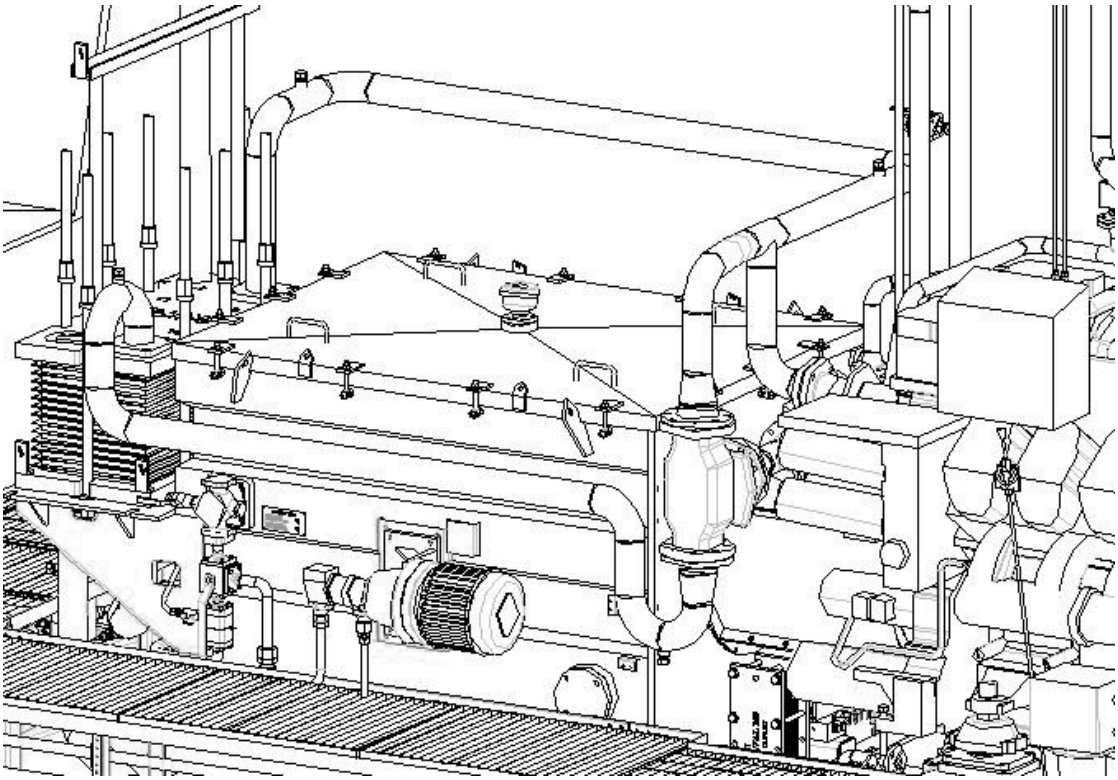

Fig. 1.4: 3D drawing of the hydraulic power unit

The HPU has 9 pistons introducing yet another harmonic load at 262,5 Hz. It is mounted directly on the skid, and it is coupled to the engine with a flexible coupling. The specific coupling in specified later in this section.

Booster pump

Manufracturer:	FRAMO
Power:	609 kW
Weight (wet):	(2000+1000)=3000 kg
Rotational frequency:	29,2 Hz

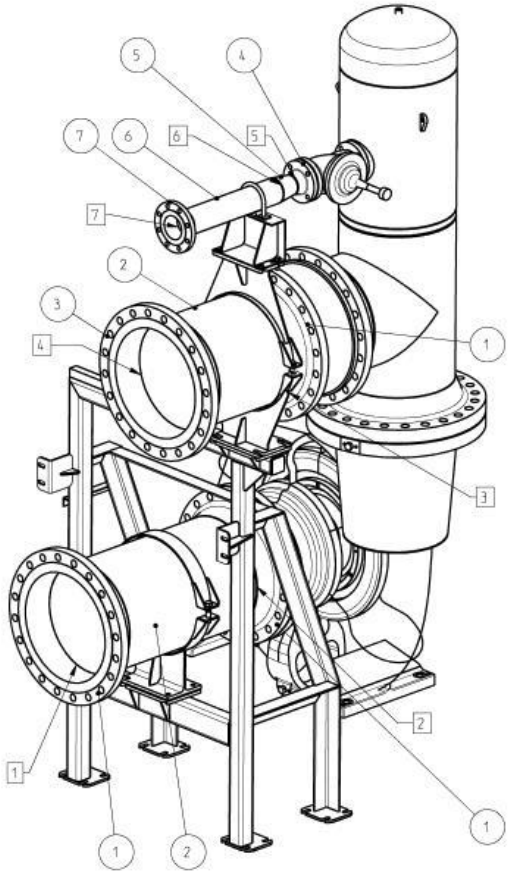

Fig. 1.5: 3D drawing of the booster pump

The PB is also mounted directly on the skid and coupled to the engine with a flexible coupling (specified later in this section). It is an impeller pump and both the shaft and impeller is utterly balanced, hence the PB is not expected to cause much vibrations.

The engine's anti vibration mount

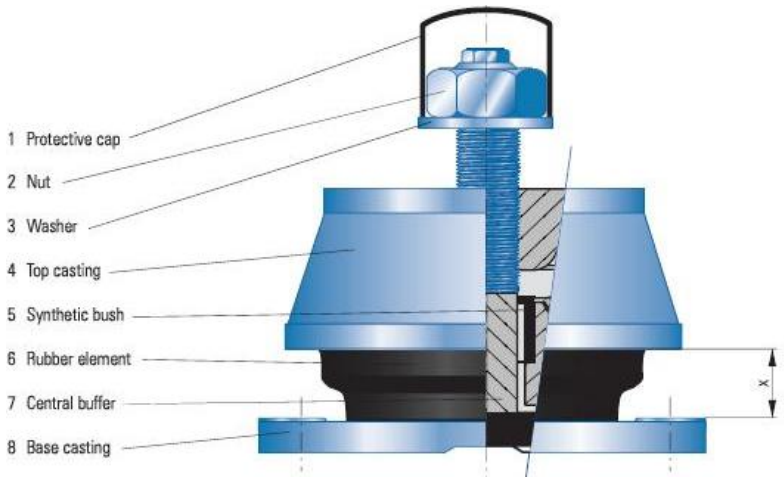

Fig. 1.6: The AVM used underneath the DE. Type RD 314 with Shore A 60 °

As mentioned earlier the engine is mounted on four AVMs, the particular type is RD314 with Shore A 60° which is illustrated in figure 1.6. I managed to obtain the documtation from the supplier, RubberDesign [12].

In figure 1.7 the vertical load is plotted against deflection for the RD314 damper. RubberDesign have equivalent graphs for all their dampers. After choosing the right damper, the angle of the shore is the degree of freedom to influence the stiffness. As one can see in figure 1.7, the AVMs used underneath the DE are the second stiffest alternative of its type. The stiffness is slightly non linear as it increases with the load. However, a rough estimate can be given;

Blue line: $\hat{k}_v = \dfrac{(7,5-0)kN}{(1,7-0)mm} = 4,4N/m$

Red line: $\check{k}_v = \dfrac{(42,5-35)kN}{(8,8-7,4)mm} = 5,4N/m$

The actual static stiffness should be somewhere in between these values.

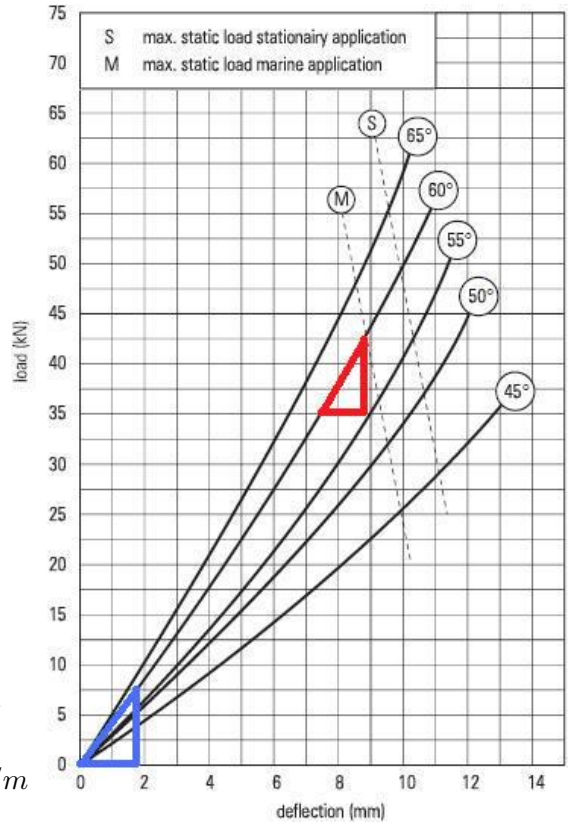

Fig. 1.7: Vertical load / deflection

The flexible couplings

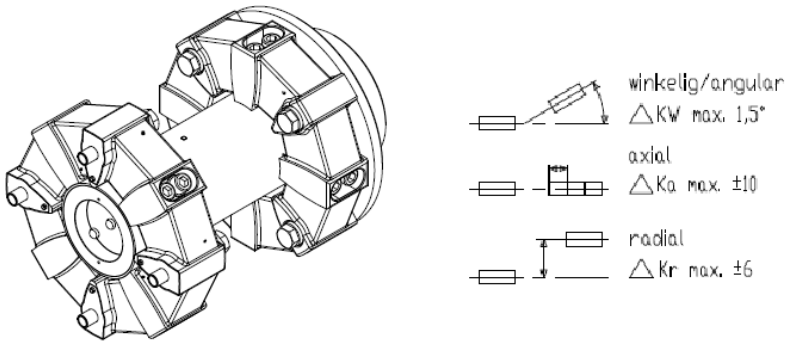

(a) 3D drawing of coupling (b) Permissible misalignment

Fig. 1.8: Flexible coupling, Centa CF A 600

Misalignment between rotating equipment generates huge dynamic forces. In this case the engine is allowed to drift since it is mounted on AVMs. This prevents it from being perfectly aligned with the HPU and the PB. The problem is solved with flexible couplings. Thus, the stiffness of the dampers and couplings are dependent.

Both of the flexible couplings are of the type Centa CF A 600, which are illustrated in figure 1.8(a). Figure 1.8(b) is extracted from the respective documentation and it describes this coupling's permissible misalignment; Centa have different specifications for all their different couplings. However, there are more factors that influence the choice of couplings than the permissible misalignment;

- The start up frequency

  This machinery only starts up once a week, hence this is a negligible factor.

- The running frequency

  29,17Hz is a high frequency for this coupling. This is a significant factor.

- Pulse factor

  The sea water lift pump starts aggressively with full engagement. This is a significant factor.

- Temperature

  Temperature affects the stiffness and size of the rubber, but this is a negligible factor in this case.

Although this thesis is not going to cover couplings in detail it is important to have a general understanding of the limitations they are introducing and also to emphasize that if the permissible misalignments are exceeded, excessive vibrations will occur.

2. THEORY

Most of the relevant theory for this thesis is described in my previous paper written last semester [14]. Yet some more theory should be discussed before executing the following analysis. As in the previous paper I am still sympathizing with discrete formulas since I am mainly using numerical approaches. This thesis presumes general knowledge of structural dynamics and numerical methods.

2.1 Root Mean Square

To calculate the *RMS* in the frequency domain, *Parseval's theorem* is used. Roughly speaking, Parseval's theorem states that the sum of the square of a function is equal to the sum of the square of its Fourier transformed;

$$\sum_n x^2(t) = \frac{\sum\limits_n |X(f)|^2}{n}$$

where $X(f) = FFT\left[x(t)\right]$, and n is number of samples

Such that the RMS calculated in time domain is the same as in frequency domain:

$$RMS = \sqrt{\frac{1}{n}\sum_n x^2(t)} = \sqrt{\sum_n \left|\frac{X(f)}{n}\right|^2} \tag{2.1}$$

The RMS of a response spectrum typically represents the energy associated with the respective vibration. It is a good quantitative measure for vibration, but it does not give any information about the occurrence of specific frequencies .

RMS is especially useful when variables are both positive and negative (e.g. we are referring to the supply voltage of 230V, which is the RMS value. The amplitude of the alternating voltage is 325V).

It is common practice to express vibrations in RMS in legislative literature. Another common measure for vibrations are "peak to peak value", which is more frequently used in older standards. These measures are illustrated in figure 2.1. Equation 2.2 describes the ratio between the amplitude and the RMS value for harmonic waves.

$$RMS = \sqrt{\frac{\int\limits_0^{2\pi} \sin^2(\omega)}{2\pi}} = \frac{1}{\sqrt{2}} \tag{2.2}$$

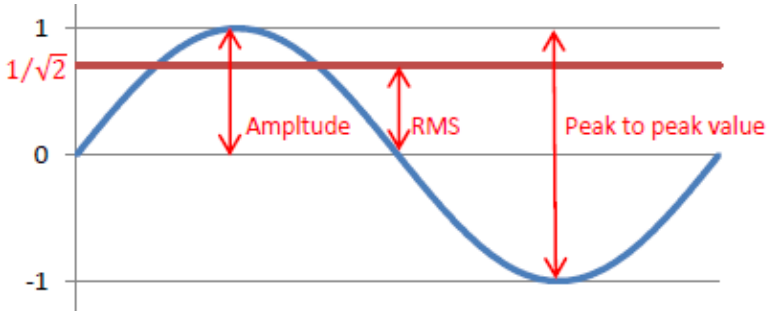

Fig. 2.1: Different ways to express the magnitude of a sine wave

2.2 Excitation Forces

It is obvious that if an engine is running at 1750rpm it will generate harmonic load at a frequency of 29,2 Hz. Harmonic loads at any multiples of this frequency will also occur and this is what is referred to as *higher order harmonics*. This is true for all rotating equipment, but for a combustion engine the combustion itself will generate vibrations on half the operational frequency and its multiples. This is because the combustion takes place in every second cycle. This is illustrated in figure 2.2.

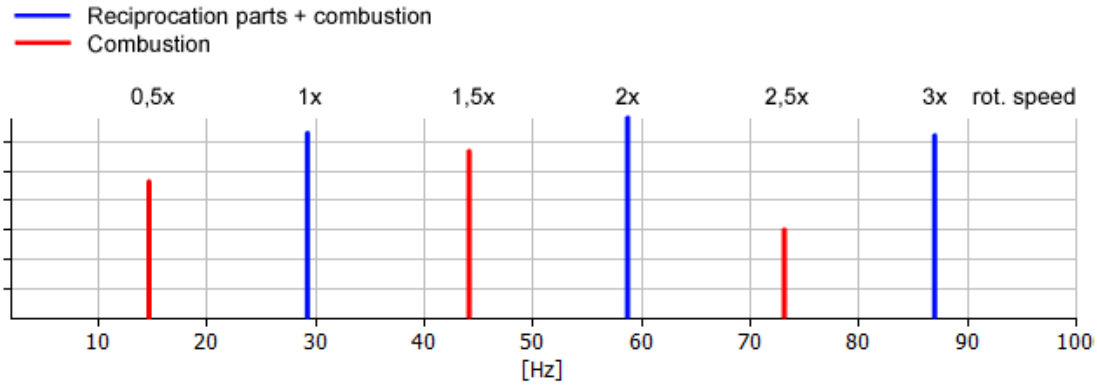

Fig. 2.2: Typical excitation forces due to a diesel engine

Typically, as the order of harmonics increase, the magnitudes decrease. Figure 2.2 is inspired by VibraTec [17] and Taylor [16].

It is normal practice to characterize the vibrations caused by a combustion engine in to two categories; torsional vibrations and unbalance vibrations.

2.2.1 Torsional vibrations

The torsional vibrations are caused by the firing strokes of the cylinders twisting the crankpin ahead of the rest of the crankshaft. When the force recedes, the crankpin tends to flex back. This behaviour is what generates vibrations illustrated in figure 2.3.

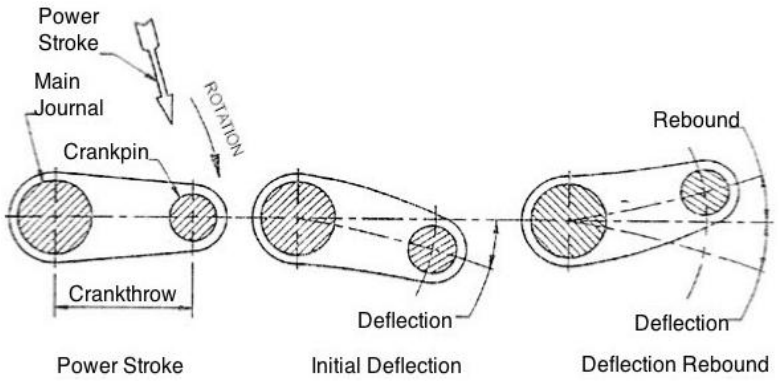

Fig. 2.3: The origin of torsional vibrations in the crank shaft

The crankshaft vibrations are considered significant since it is many cylinders, which leads to a long crankshaft, which again leads to a flexible shaft.

2.2.2 Engine unbalance vibrations

In theory, a V16 engine is perfectly balanced regardless of the V angle due to symmetry. However, some vibrations due to unbalance are expected, for instance because the shafts are not perfectly balanced.

2.3 Dampers

There are various solutions for excessive vibration. When the vibrations are associated with the machinery's main functions, as in this case, the easiest way to deal with it is to reduce the vibrations by damping. This section describes some pertinent damper solutions.

2.3.1 Passive damper

A passive damper is the traditional damping foot (AVM), which is already mounted underneath the DE, see figure 1.6. The damper is mounted between the vibration source and the supporting surface and absorbs the kinetic energy of the vibration.

- Advantages of passive dampers

  Well researched

  Easily installed

No moving parts

Cheap

- Disadvantages of passive dampers

  Limited to a fixed frequency band

  Enables more drifting of the structure

It is not favourable to make the equipment support too soft. Low frequency loading or static forces due to static unbalance could push the equipment out of line and therefore create even more vibrations. On the other hand, since the engine is coupled to both the HPU and PB with flexible couplings, this is justifiable within the permissible misalignment of the coupling.

2.3.2 Active mass damper

The principle of an active mass damper is to cancel out the vibration by creating a counteracting force generated by a moving mass at a counter phase with the vibration source.

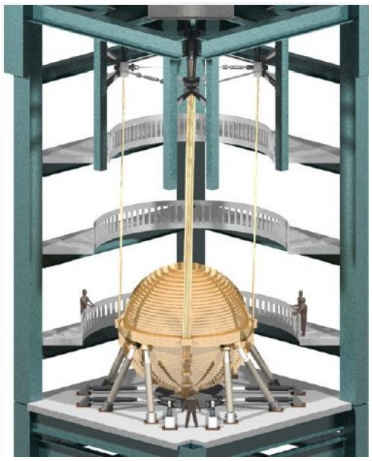

Fig. 2.4: TMD in Tapei 101

Tuned mass damper

The TMD is the simplest form of an active mass damper, typically used in tall towers. The idea of the TMD is to attach a small mass (relative to the vibrating mass) and tune it (by manipulating the eigenfrequency) in such a way that it dampens vibrations in a certain band-with. This is described more detailed in section 5.2.3.

The TMD in figure 2.4 is one of the largest TMDs in the world, it is 730 tons and located between 87th to 91st floor of Tapei 101.

Harmonic damper

This is a very simple form of TMD, although it does not contain any moving parts, it is a moving part. It is fixed to the crank shaft, and serves no other purpose than damping the torsional vibrations in the crank shaft.

The damper has two main parts; a mass and an energy dissipating element. The mass creates momentum which resists the acceleration of the vibration, and the energy dissipating element (fluid/rubber) absorbs the vibrations. The energy dissipating element is a wear part and needs to be replaced due to wear. I am assuming this is already implemented to the current crank shaft.

Fig. 2.5: Harmonic damper

Actuator

The actuator is based on the principle that accelerating a suspended mass results in a reaction force on the supporting structure. It is a sophisticated way of cancelling out vibration at certain frequencies by accelerating the mass in the TMD with for instance an electromagnet. The implementation of an actuator is described more detailed in section 5.2.4.

- Advantages of active dampers

  Precisely cancels out fixed frequencies

- Disadvantages of active dampers

  Delicate, error could cause fatal resonance/amplification

  Introduces additional mass/force

  Increased number of moving parts

  Cumbersome installation

  Needs maintenance

Active mass dampers are also a widely used damping solution, for instance almost every modern car have at least one active mass damper, some may have ten or more. The machinery runs at a fixed rotational velocity and therefore this is a tempting solution.

2.3.3 Semi-active damper

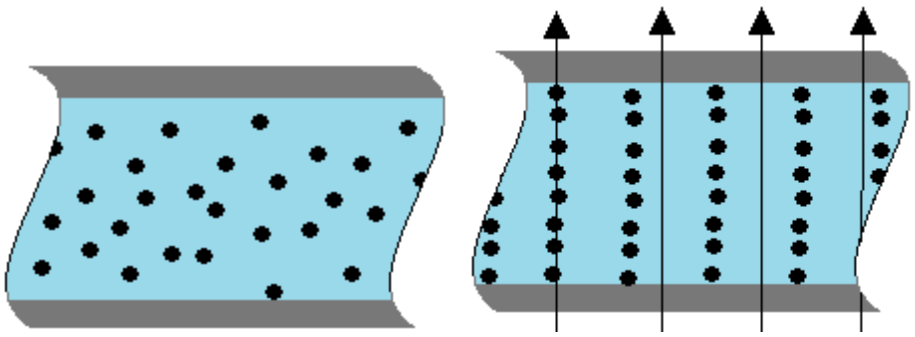

(a) Magnetic particles distributed randomly in fluid

(b) Magnetic particles aligned along the lines of a magnetic flux

Fig. 2.6: Principle of MR fluid

The *magneto-rheological* damper is a semi-active damper based on oil containing metal particles and an electromagnet. When a magnetic field is applied to the MR fluid it becomes stiff because the metal particles are aligned. This allows the characteristics of the damper to be continuously controlled by varying the power of the electromagnet.

- Advantages of semi-active dampers

  Small size

  Few moving parts

  Reacts dynamically to a number of vibration frequencies

- Disadvantages of semi-active dampers

  Delicate

  Limited research available

  Expensive

Because of its small size, the magneto-rheological damper can be installed in combination with the traditional passive damper, which allows one to combine the best of both worlds.

2.4 Composite materials

Composite materials are materials made from two or more different materials. The ones discussed in this thesis consists of fibres and matrix. The matrix has low strength but keeps the fibres fixed. Typical types of matrix are thermoplastics, ceramics or thermosets, the latter will be considered here. Typical fibres are kevlar, boron, carbon and glass, the last two types will be considered here. Carbon has a very high stiffness which makes it good for dynamic problems. This will be emphasized in section 2.5. The matrix and fibres can be combined in different ways and this thesis is going to study the case where the fibres are continuously aligned forming an orthotropic ply. Orthotropicity implies that the ply have different properties in the 1– and 2-direction, where the 1-direction corresponds to the axis parallel to the fibres and the 2-direction is the perpendicular axis.

The following data is extracted from matweb [1] and Dharan [7].

Tab. 2.1: Typical material properties

	Density [kg/m^3]	*Youngs modulus* [GPa]	*Price* [NOK/kg]
Matrix			
Epoxy resin	1,25	4,5	10
Polyester	1,35	3,5	6
Fibre			
S Glass	2,46	84	10
HM Carbon	1,8	350	200

2.4.1 Tailoring composites

Composite materials allows one to tailor the material, first by choosing the proper fibres and matrix forming a ply, and secondly by mixing plies with different orientation or of different materials to get the desired properties. I will make two different plies by combining some of the materials in table 2.1. For this to be accomplished some mathematical derivations are needed:

E in the 1-direction mixes linearly: $$E_1 = v_f \cdot E_f + (1 - v_f) \cdot E_m \tag{2.3}$$

Combining this with Hookes' law gives: $$\frac{1}{E_2} = \frac{v_f}{E_f} + \frac{v_m}{E_m}$$

Hence: $$E_2 = \frac{E_f E_m}{E_m v_f + E_f(1 - v_f)} \tag{2.4}$$

Where v_f is the volume fraction on fibre in the composite. The price and density obviously mixes linearly.

Tab. 2.2: Strength properties of some composite laminae, $v_f = 0,6$

Composite	E_1 [GPa]	E_2 [GPa]	*Density* [kg/m^3]	*Price* [NOK/kg]
S Glass - Epoxy	52,2	10,4	1976	10
HM Carbon - Epoxy	211,8	11,0	1580	124

Combining laminae to make the desired material is further elementary matrix algebra, since it is not needed for the later conclusions, it is not included in this thesis.

2.5 Dynamic material index

Material indexes are used to compare materials in a systematic way. By defining an index which reflects the properties that are important, numerous materials can be compared with quick calculations. Since vibrations will be studied it is natural to compose a simple material index regarding dynamics; A square cantilever beam with fixed length is subjected to harmonic longitudinal load on the tip, figure 2.7. The structural damping is also neglected.

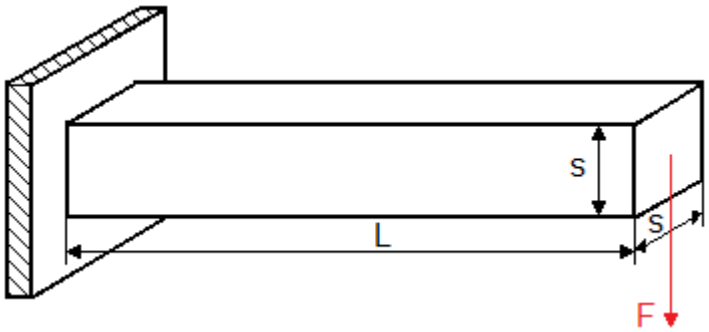

Fig. 2.7: Square cantilever beam subjected to load at the tip

The mass of the beam is:	$m = L \cdot s^2 \cdot \rho$
Deformation due to a static load would be:	$\Delta L = \frac{L \cdot F}{s^2 \cdot E}$
Hence the longitudinal stiffnes is:	$k = \frac{s^2 \cdot E}{L}$
Assuming linear deformation, eq'n of motion becomes:	$\frac{m}{2} \cdot \ddot{r} + k \cdot \mathrm{r} = F\cos(\overline{\omega})$
This gives the following eigenfrequency:	$\omega_n^2 = \frac{k}{m} = \frac{E}{2L^2 \cdot \rho}$
The final response becomes:	$\mathrm{r} = \frac{F}{k\left\lvert 1 - \left(\frac{\overline{\omega}}{\omega_n}\right)^2\right\rvert} \cdot \cos(\overline{\omega})$
Thus, the dynamic amplification is:	$D = \frac{1}{\left\lvert 1 - \left(\frac{\overline{\omega}}{\omega_n}\right)^2\right\rvert}$ (2.5)

From a mathematical standpoint, to minimize the dynamic amplification (eq. 2.5) either make sure $\omega_n < \frac{\overline{\omega}}{\sqrt{2}}$ and minimize ω_n, or simply maximize ω_n.

From a dynamical standpoint the first approach is not very practical, it is only possible if it is a very long beam subjected to purely high frequency load, and it would make a very unstable system. The only proper approach is to maximize ω_n. To maximize ω_n, $\frac{E}{2L^2\rho}$ have to be minimized, and since $2L^2$ is a constant in this case it means to maximize the ratio $\frac{E}{\rho}$. The material index becomes;

$$i = \frac{E}{\rho} \tag{2.6}$$

This material index, eq. 2.6, is a very typical index for dynamic optimization. It is intuitive that high stiffness (which resists motion) and low mass (which generates momentum) are good material qualities from a dynamic point of view.

From this index it is quite obvious that one should choose a carbon composite in table 2.2. However, the price would probably acknowledge the opposite. To minimize

cost, the density, ρ, can be replaced by $C_m\rho$ where C_m is the cost per kg. To obtain more definite material indexes, more information about the actual problem is needed.

Table 2.3, is extracted from Ashby [3] and Cebon [4].

Tab. 2.3: Dynamic material indexes

Function and constraints	*Maximize*
Ties, columns	
maximum longitudinal vibration frequencies	E/ρ
Beams, all dimensions prescribed	
maximum flexural vibration frequencies	E/ρ
Beams, length and stiffness prescribed	
maximum flexural vibration frequencies	$E^{1/2}/\rho$
Panels, all dimensions prescribed	
maximum flexural vibration frequencies	E/ρ
Panels, length width and stiffness prescribed	
maximum flexural vibration frequencies	$E^{1/3}/\rho$
Ties, columns, beams, panels, stiffness prescribed	
minimum longitudinal excitation from external drivers, ties	$\zeta E/\rho$
minimum flexural excitation from external drivers, beams	$\zeta E^{1/2}/\rho$
minimum flexural excitation from external drivers, panels	$\zeta E^{1/3}/\rho$

Where ζ is the damping coefficient (loss coefficient).

2.6 Vibration criteria

Vibrational issues are a rising concern in the offshore industry. A lot of different standards are enforced depending on where in the world the installation is located. Since FRAMO is a worldwide company they have to stay updated to meet all the standards. There are three main concerns that will be discussed in this section; vibration regarding the equipment itself, human exposure of whole-body vibration and human exposure of noise.

2.6.1 Vibration regarding the equipment itself

Amongst other places, this is described in ISO 10816. The typical frequency range of interest is 2-1000 Hz, and the quantity of interest is RMS velocity (m/s). The criteria regarding the current equipment is well derived in section 3.1. Traditionally this has been

the most emphasized concern regarding vibrations, and it is obviously a prerequisite that the machinery works in order to appraise the other criteria.

2.6.2 Human exposure of whole-body vibration

Amongst other places, this is described in ISO 6954. The typical frequency range of interest is 8-80 Hz, and the quantity of interest is RMS velocity (m/s).

According to Griffin [9], at very low frequencies (less than 0,5 Hz) the vibrations are associated with motion sickness and this is not of any concern in this case. For frequencies above 80 Hz the seated, standing or recumbent body is usually well isolated from vibration.

This could be an issue because the vibrations from the FWP module is conducted to the deck causing hull vibration. The low frequency range is also an important aspect regarding structure-born noise.

2.6.3 Human exposure of noise

Amongst other places, this is described in ISO 9614. The typical frequency range of interest is 20-20000 Hz, and the quantity of interest is sound pressure level (dB). Table 2.4 describes different offshore noise limits which are slightly higher than onshore noise limits.

Tab. 2.4: Recommended offshore noise limits from BV 4247

Specific work areas of offshore Installations	*Noise limit* [dBA]
General work area	88
Workshops	70
General stores	70
Kitchens	60
Control rooms	55
Offices	55
Laboratories	55
Communication rooms	45

These limits generally apply for broad band noise. If a noise exhibits dominant tonal characteristics then it may be desirable to suppress such characteristics [11]. The generalized limits in table 2.4 corresponds to specific limits within smaller frequency bands in the spectrum, but this thesis does not go in any further detail on this topic.

I have not measured any sound intensity, and this issue is not directly a part of my thesis, but for the completeness the subject is still mentioned. Vibrations and noise are directly dependent and by limiting vibrations the noise will be decreased.

3. FACTORY ACCEPTANCE TEST

In January I spent some days at the test facilities at FRAMO. I participated in a couple of different tests regarding the fire water pump module. My thesis is limited to the dynamic response in normal operation and the test which is most pertinent is the one presented in this chapter. Still some other tests will be mentioned where it is appropriate.

Different people were involved in the test events, but I was mostly collaborating with Ørjan Vatsøy at Frank Mohn Flatøy A/S and supervised by the head of the technical department, Sigve Gjerstad.

To measure the response of the system due to *internal loads*[1] we used hardware (sensors, signal processing module etc.) provided by *VibraTec* and software provided by *Brüel & Kjær*.

3.1 Acceptance criteria

The vibrations on the equipment described in section 1.3 should be within ISO[2] and API[3] standards, described in table 3.1.

Tab. 3.1: Limiting vibration criteria

Equipment	*Upper RMS value*	*Frequency range*	*According to*
PB	3.0 mm/s *	[5-1000 Hz]	API 610
DE	28.2 mm/s	[2-1000 Hz]	ISO 10816-6 (Class 5 machine)
HPU	17.8 mm/s	[2-1000 Hz]	ISO 10816-6 (Class 4 machine)
Base plate	7.1 mm/s **	[2-1000 Hz]	ISO 10816-6 (Class 2 machine)

* Below 2.0 mm/s at a discrete frequency.

** Except on the FWP support points where the global RMS levels must be restricted to 3.0 mm/s. At the HPU support points may the overall velocity level in some cases be between 7.1 and 17.8 mm/s RMS.

To ensure that the vibrations are within the criteria, FRAMO have defined some standard measuring positions on the FWP module which are illustrated in figure 3.5(a) and 3.5(b).

[1] Loads generated by the system itself

[2] International Organization for Standardization

[3] American Petroleum Institute

3.2 The set-up

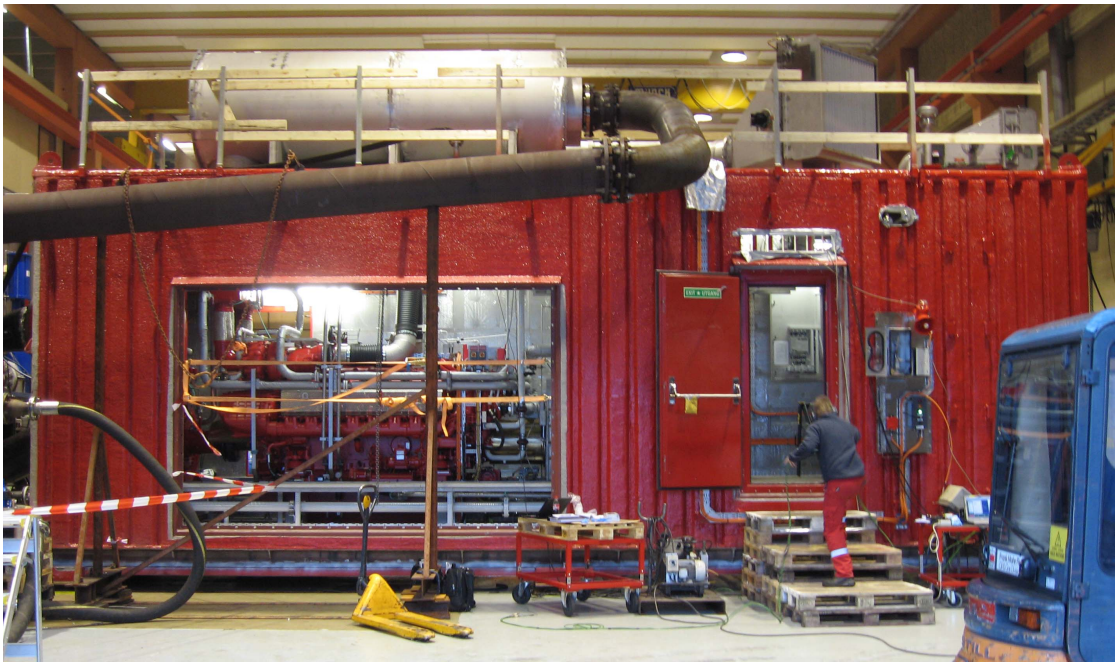

Fig. 3.1: Overview

The module is connected to a *test loop* which implies that it is pumping seawater from a tank through a loop of pipe stacks and back to the tank. By configuring different valves the suction pressure can be manipulated to simulate different water depths.

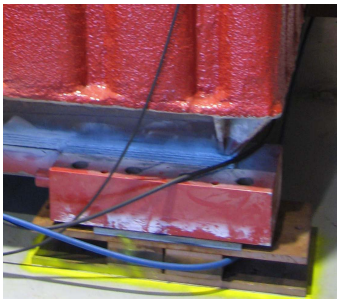

The module is resting on *VibraTec elastic pads* (see figure 3.2), consisting of two rubber elements that are coupled in parallel. The pads have a certain stiffness and damping in order to simulate the effect of being placed on the deck of a ship rather than on the concrete floor. The feet are customized for this particular case[4] since the parameters will vary on different ships and rigs.

Fig. 3.2: Elastic pad

The system is running through all of the dynamic tests, except one; This test implies measuring the eigenfrequencies by striking the module with an impact hammer and Fourier transform the impulse response to visualize the eigenfrequencies.

[4] Clov, Angola

The vibration is picked up by *velometers*[5] and *accelerometers*[6]. Figure 3.3 shows how such probes are mounted to monitor the vibrations. These probes are mounted stationary during the whole test. The data are continuously analysed in the control room in fig. 3.4.

The temperature, pressure and flow between every element in the loop are continuously monitored in the control room. The vibrations are also monitored and plotted against time, flow and frequency in all three axes. The latter is obtained by a continuously FFT[7] analysis of the vibrations to get the response spectra in the different axes. This helps the experienced supervisor to detect potential threats. Excitation of certain frequencies may coincide with a scratch in the bearing raceway or other deviations.

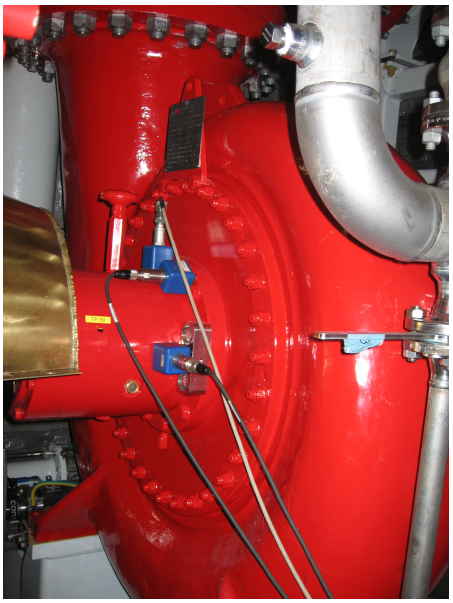

Fig. 3.3: Velometers mounted on the PB

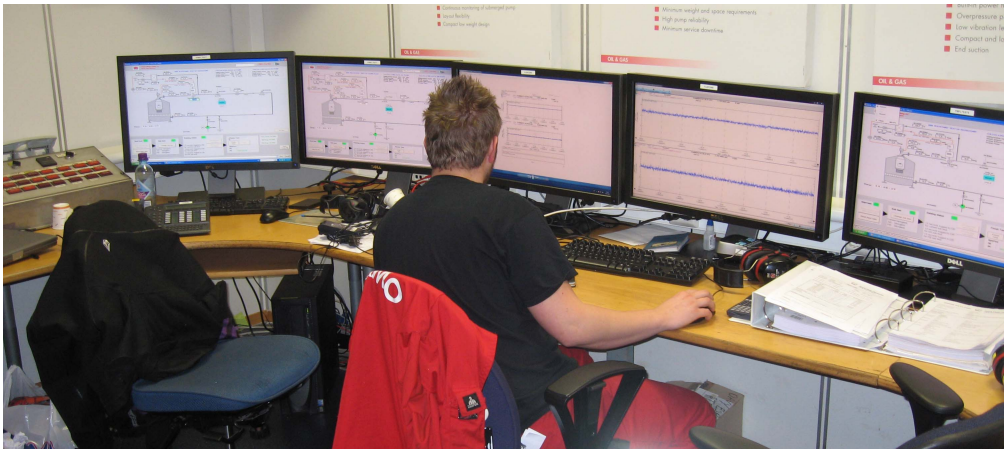

Fig. 3.4: Ørjan Vatsøy supervising the vibrations in the control room

[5] Probes that measures velocity
[6] Probes that measures acceleration
[7] Fast Fourier Transform

3.3 Determining the response

To gain a better understanding of the dynamic response of the system a more comprehensive dynamic test is executed using two velometers which picks up vibrations in all three axes. The first velometer is fixed at an anchor point on the skid, figure 3.7(a). The second velometer is moved around on tactical locations on the module, figure 3.7(b).

In figure 3.7(b) I am mounting it beneath the diesel engine (position 16 on fig. 3.5(b)).

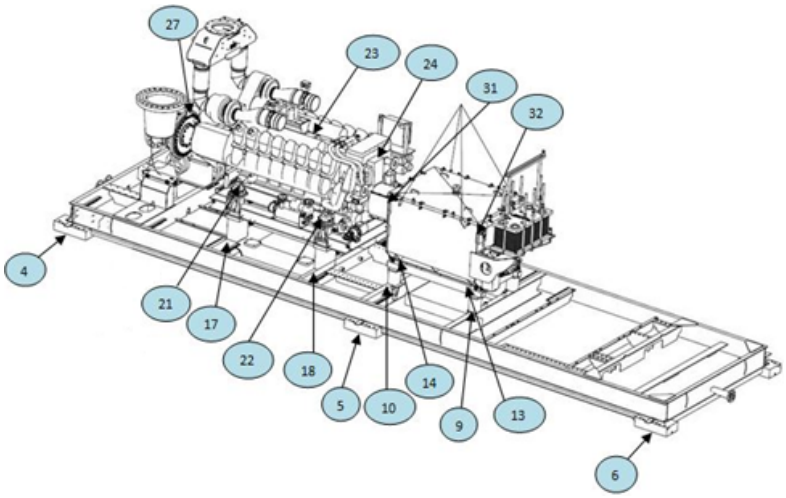

(a) Skid seen from the “right” side

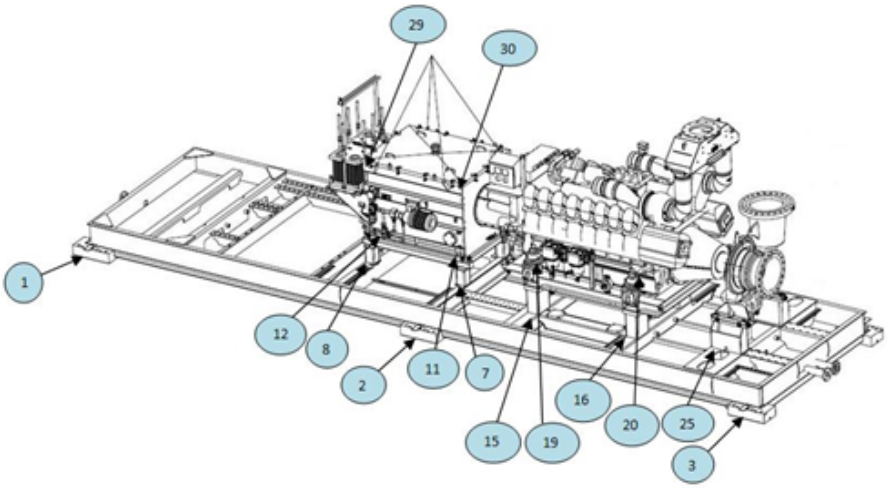

(b) Skid seen from the “left” side

Fig. 3.5: Measuring positions

The measuring positions illustrated in figure 3.5(a) and 3.5(b) are defined to obtain a complete overview of the response for each piece of equipment in the module and for the skid. This is done to make sure that the vibration levels on the equipment are within the limits specified in ISO and API standards. With origin in these standards, FRAMO have defined tolerances for the RMS velocity in different frequency ranges for all of these positions [2].

3.3.1 Preparing the software

The software has to be programmed to fit this particular task. All the positions that are going to be measured have to be defined relative to the anchor point. In addition, the relationships between the locations have to be described giving the simple grid model in figure 3.6.

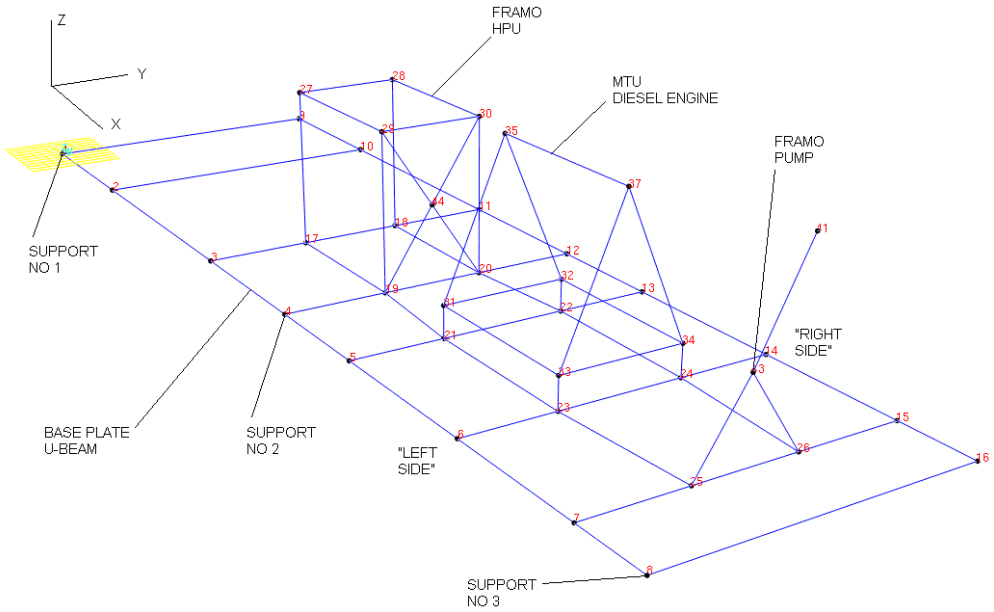

Fig. 3.6: Grid model

3.3.2 Gathering data

(a) Fixed probe (b) Movable probe

Fig. 3.7: Determining the dynamic response of the system experimentally

The movable probe measures the vibrations for 40 seconds in every position. The signal is analysed by a computer and further response spectra, in all three axes, are generated for every position. In addition to save the vibration data, the RMS velocities of the different points are checked to assure that they are within their respective tolerances, see table 3.1.

3.4 Results

The software created a response spectrum for all the measurement positions and the RMS velocity is calculated by summing over the frequency ranges described in section 3.1.

As table 3.2 shows, all the values are within the acceptance criteria. This is sufficient for the normal dynamic analysis (FAT[8]).

[8] Factory Acceptance Test

Tab. 3.2: Test results

#	Direction of measurement			Description
	Axial (x)	Transverse (y)	Vertical (z)	
	RMS (mm/s)	RMS (mm/s)	RMS (mm/s)	
1	0.9	0.9	0.8	Skid - Support points
2	0.9	1.4	1.7	
3	0.8	1.4	0.9	
4	1.2	1.2	1.1	
5	2.0	2.4	1.7	
6	1.2	0.9	0.9	
7	6.5	2.5	4.6	Skid - HPU support
8	4.4	2.8	4.2	
9	7.7	2.5	3.2	
10	6.9	2.4	6.9	
11	5.4	8.2	4.1	HPU - Bottom
12	7.6	13.7	3.8	
13	9.1	15.4	4.3	
14	10.1	11.2	7.0	
15	0.970	1.5	2.1	Skid - Engine support
16	1.6	1.5	1.9	
17	1.1	1.5	2.2	
18	1.5	1.5	2.0	
19	7.5	8.9	5.8	Engine - Bottom
20	7.7	9.7	7.3	
21	6.0	10.8	7.9	
22	6.8	23.7	19.2	
23	12.2	28.0	12.7	Engine - Top
24	8.0	10.4	6.8	
25	1.1	1.2	1.6	Skid - PB support
26	1.3	1.3	1.5	
27	2.5	1.8	1.7	PB - Bearing housing
29	11.4	15.5	15.5	HPU - Top
30	6.6	12.8	5.7	
31	9.5	14.3	10.6	
32	16.8	10.8	12.5	
33	5.7	13.3	3.6	HPU

4. MINIMIZING THE VIBRATION LEVEL IN THE SUPPORT POINTS

4.1 Identifying the nuisance

To minimize the structure-born noise the vibration level in the support points has to be minimized. Finding the main contribution of vibration is the first natural step to achieving this goal. In this case there are three sources of vibration; the PB, the DE and the HPU.

4.1.1 Averaging the RMS

The values from table 3.2 are averaged and arranged geometrically in table 4.1.

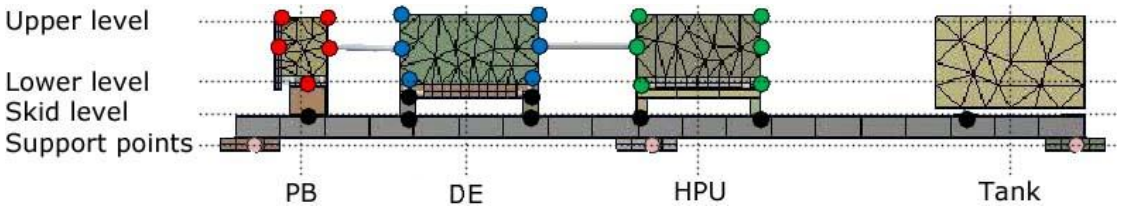

Fig. 4.1: Illustration of the geometry in table 4.1

Tab. 4.1: RMS velocity [m/s] averaged and arranged geometrically

	PB			*DE*			*HPU*			*Tank*		
	x	y	z	x	y	z	x	y	z	x	y	z
Upper level				10,1	19,2	9,7	11,1	13,3	11,1			
Lower level	2,5	1,8	1,7	**7,0**	13,3	10,0	**8,0**	12,1	4,8			
Skid level	1,2	1,3	1,5	**1,4**	1,5	2,0	**6,4**	2,5	4,7			
Support pt's	1,0	1,3	1,0				1,5	1,9	1,7	1,0	0,9	0,8

The vibrations increase further away from the skid (where it is supported). An interesting observation is that the DE vibrations does not propagate to the skid in the same way that the HPU vibration does. This is because the DE is mounted AVMs, whereas

the HPU is not. This indicates that the HPU represents the greatest contribution to the skid's RMS velocity. An evident suggestion would therefore be to mount the HPU on AVMs as well. This suggestion will be investigated in section 5.1.

4.1.2 Looking at the response spectra

Recall the excitation frequencies from section 2.2. In addition to the engines excitation forces, it should also be kept in mind that the HPU has 9 pistons and therefore introduce a high frequency load at

Piston frequency:	$9 \times 29,17 \text{ Hz} = 262,5 \text{ Hz}$
2nd order harmonic:	$2 \times 262,5 \text{ Hz} = 525 \text{ Hz}$
3rd order harmonic:	$3 \times 262,5 \text{ Hz} = 787,5 \text{ Hz}$

I have made another figure similar to fig 2.2, but here the harmonic load of these pistons in addition to its higher order harmonics have been included. Section 4.1.1 indicated that the HPU influences the response spectrum considerably, so these frequencies are good to keep in mind.

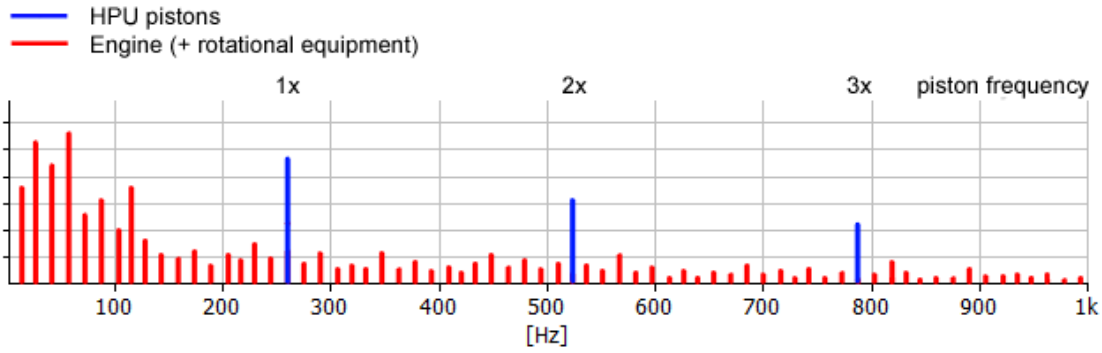

Fig. 4.2: Theoretical excitation frequencies

In the following plots the response spectra for the vibration sources have been plotted in the same figure as the response spectra for the skid in the respective equipment support. This is an attempt to reveal how much of the vibration that propagates to the skid.

Conclusively the response spectra for the support points are plotted in anticipation of revealing the distinctive vibration source.

The DE

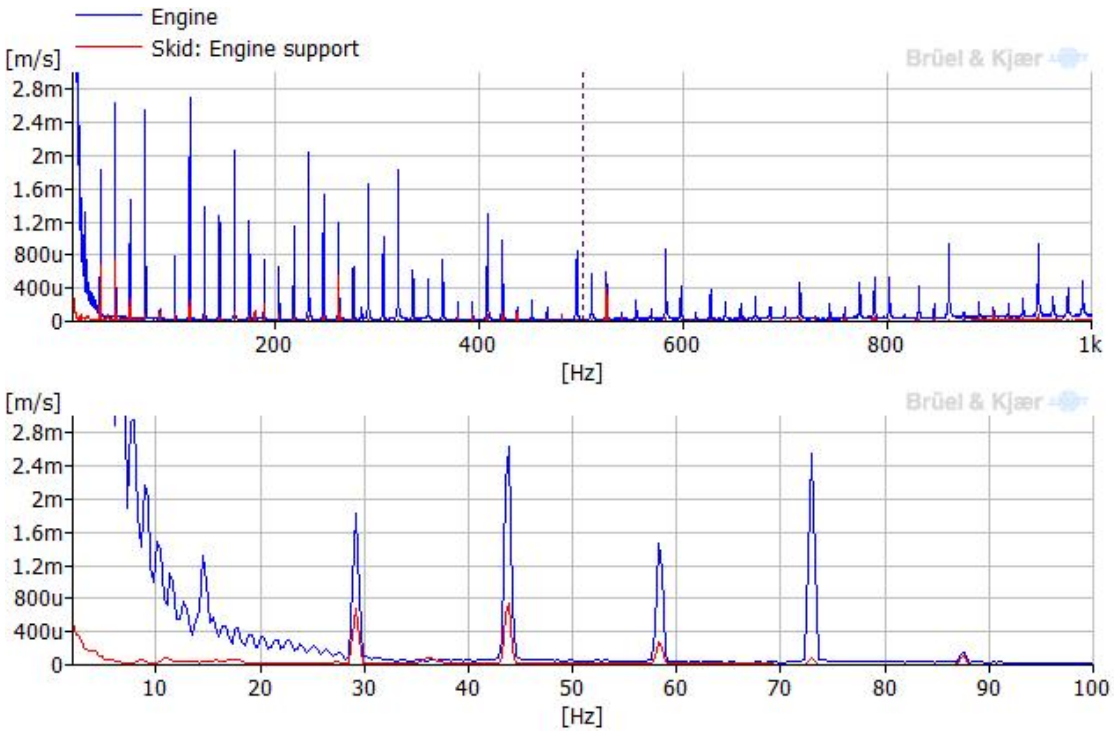

Fig. 4.3: DE, RMS velocity response spectra

Figure 4.3 clearly shows that the theory from section 2.2 corresponds to the measurements. An interesting observation is that the vibration from the elastic pads obviously absorbs a lot of the vibration. The critical points corresponds to the harmonic frequencies, which for the skid are strictly below 1 m/s.

The PB

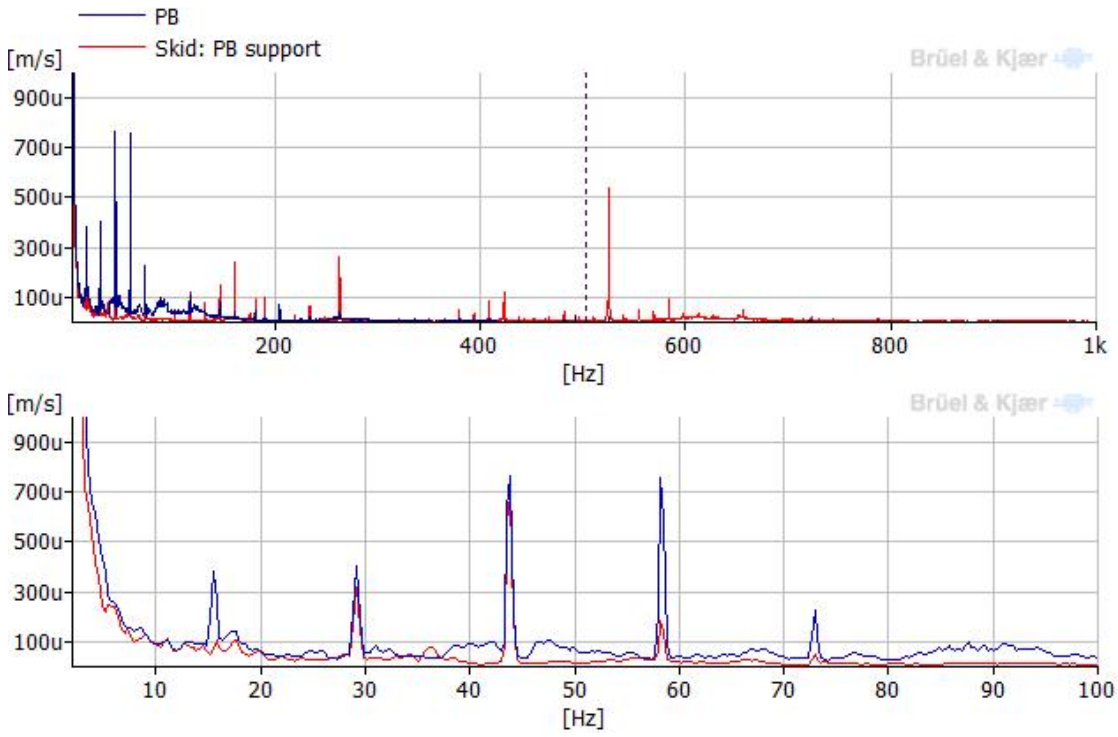

Fig. 4.4: PB, RMS velocity response spectra

The PB has the strictest acceptance criterion for vibrations and are expected to contribute least to the skid vibration. This seems to be true when looking at the response spectra. An interesting remark is that the skid is vibrating more than the PB at frequencies above 400 Hz. This could be caused by resonance, but it is more likely to be that the skid is excited by the other equipment, and that it is actually the skid causing additional vibration of the PB. Note that the peaks at 262,5 Hz and 525 Hz originates from the HPU pistons, hence the HPU vibration is conducted through the skid creating disturbance on the PB.

The HPU

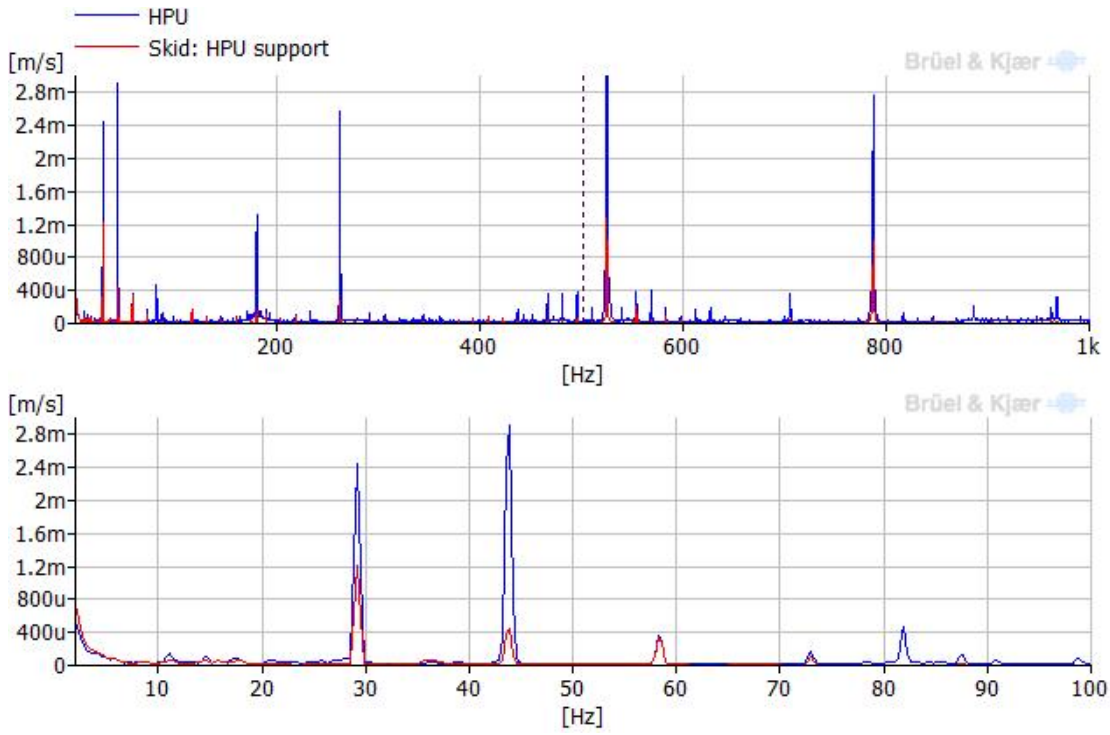

Fig. 4.5: HPU, RMS velocity response spectra

Figure 4.5 clearly match the characteristics from figure 4.2. The vibration impact on the skid does not seem to be any worse than the engine, except on the piston frequency and its harmonics. The magnitude of these peaks are five times higher then the peaks from the other equipment and definitely seem to represent a lot of the RMS velocity. This allegation will be revealed when studying the conclusive plots; the response spectra of the support points, figure 4.6.

The support points

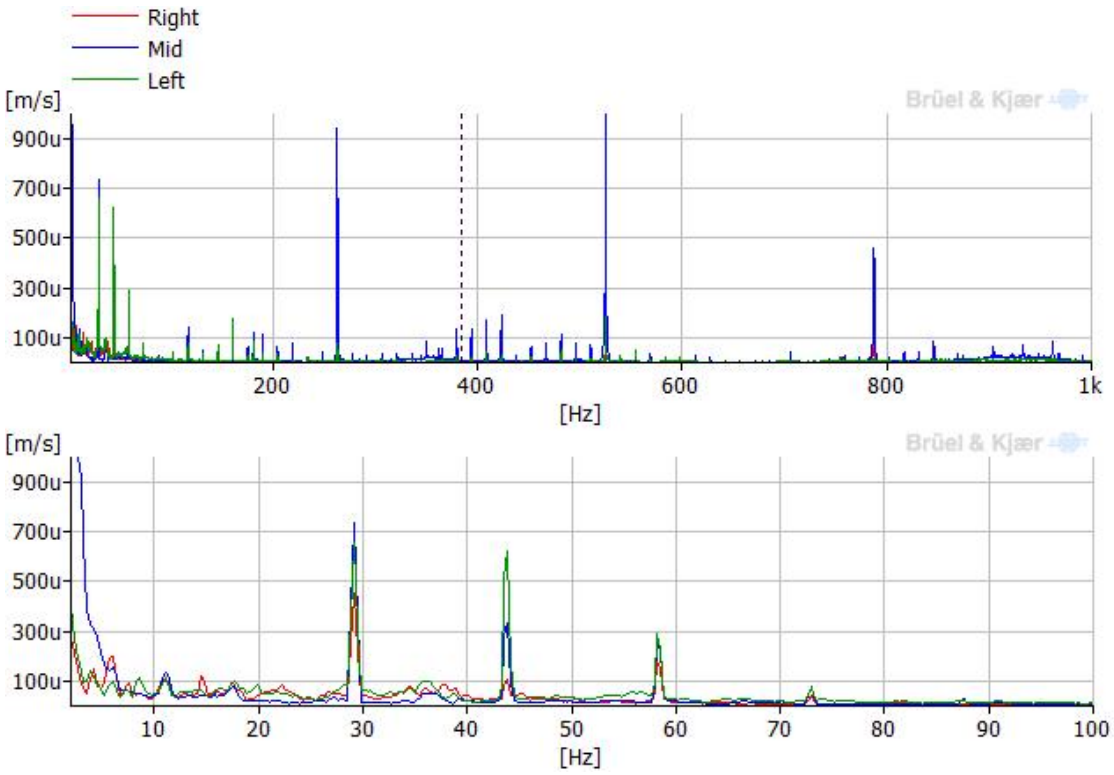

Fig. 4.6: Support points, RMS velocity response spectra

The response spectra of the support points clearly resembles those of the HPU and the peaks at the piston harmonics are truly the major peaks. The HPU seems to be causing the main dynamic loads on the deck. Note that the red graph in figure 4.6 has the least magnitude, this graph represents the module support on the right (underneath the diesel tank, see figure 4.1), in other words furthest away from the vibration sources.

4.1.3 Looking at the mode shapes

It can be convenient to look at the mode shapes to understand the behaviour of the system. *Pulse LabShop*[1] can calculate the mode shapes based on the different spectra in the locations and the geometry which is defined in section 3.3.1. Firstly, the critical frequencies are localized by looking at the response spectra for the support points, figure 4.6. The mid-section support points have been used for guidance since this is where the greatest vibrations occur. The critical points are given in table 4.2.

Tab. 4.2: Critical points in the support points response spectra, fig 4.6

Description	*Frequency* [Hz]	*Velocity* [m/s]
n	29,2	7,35E-04
$1,5 \times n$	43,8	3,34E-04
$2 \times n$	58,3	2,78E-04
N	262,5	9,45E-04
$2 \times N$	525,0	1,64E-03
$3 \times N$	787,5	4,64E-04

The mode shapes of the three most critical frequencies are studied, in other words at the DE's rotational speed, and the two first harmonics from the HPU pistons.

The mode shapes are not very clear in the pictures. For better visualisation see attached animations (appendix G).

The engines rotational speed, n

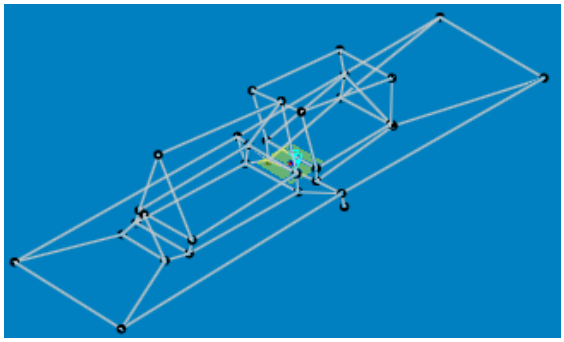

Fig. 4.7: Mode shape at 29,2 Hz

Figure 4.7 describes the mode shape corresponding to the DE frequency. The PB behaves completely rigid in this mode shape, both the DE and the HPU are vibrating in a pitch dominated shape[2]. The HPU is moving noticeably more than the DE, and the DE also

[1] The software provided by Brüel & Kjær
[2] Pitch motion = rotation about the y-axis

seems to move in counter-phase with the HPU and the skid which are moving together. This is apparently explained by the dampers on the DE.

First harmonic of the HPU pistons, N

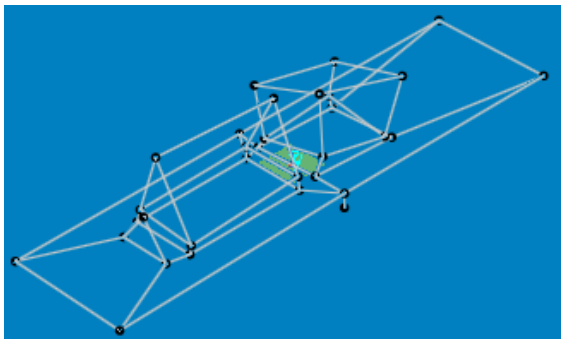

Fig. 4.8: Mode shape at 262,5 Hz

The mode shape corresponding to the HPU piston frequency is described by figure 4.8. Both the PB and the DE are acting rigid in this mode shape, although a small movement in the engine can be observed. The HPU motion is pitch dominated.

Second harmonic of the HPU pistons, $2 \times N$

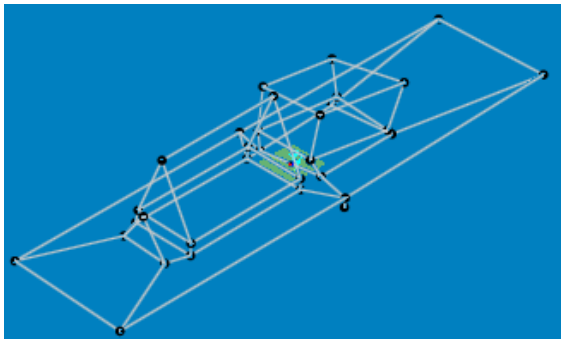

Fig. 4.9: Mode shape at 525,0 Hz

Finally, figure 4.9 describes the mode shape corresponding to the second harmonic of the HPU piston frequency. Both the HPU and the DE behave rigid, and here the DE has an even smaller motion. The HPU is also moving with a pitch dominated motion.

4.2 Suggested potential improvement

4.2.1 Dampers

To reduce the structure-born vibration it is likely that additional damping is needed. The following is a discussion about which type of damper solution that is most beneficial (recall section 2.3) and where it is needed.

Placement of dampers

Simply mounting dampers between the module support and the deck would be an easy solution, but there are some drawbacks. First of all, figure 4.4 indicates that the vibration from the HPU is conducted through the skid to the PB. It is better to damp each of the machines separately so that they do not interfere with each other. Secondly, the vibration characteristics are quite different for the different pieces of equipment therefore a more advantageous damping can be obtained with different dampers customized to each piece of equipment.

Type of damper solution

It is less obvious to determine which type of damper solution that is most beneficial. Since the DE is running with constant rotational velocity, the loading has fixed frequencies and the semi-active damper solution is rejected.

Additional passive dampers is a cheap and reasonable improvement idea. It is also possible to install on modules after commissioning. After the engineering work have been done once, it is likely to result in low installation costs.

4.2.2 Supportive beams

Making the system stiffer by introducing supportive beams could be another way of manipulating the vibrations. As studied before [14], fixing the foundation and making the above stiffer increases the eigenfrequencies, thus limiting low frequency vibrations, but potentially amplifying high frequency vibrations. If one suspect the excessive vibrations to be caused by a resonance frequency, it would be a good idea to shift the eigenfrequencies. The excessive vibrations seem to appear at the excitation frequencies and especially in the high frequencies, this refutes making the system stiffer. The pitch motion of the HPU is prominent in the mode shapes of the governing vibration frequencies and for this reason it could be tempting to prevent this motion by applying supportive beams.

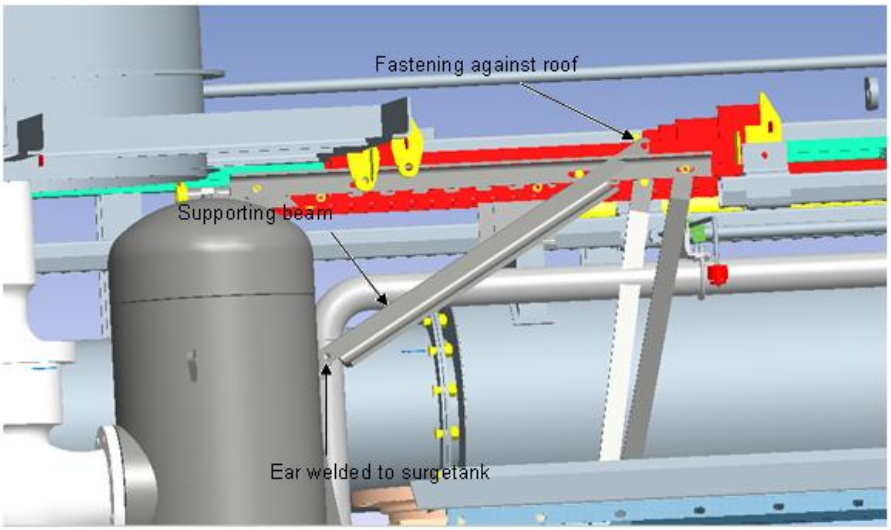

Fig. 4.10: Design modification on Pazflor

On a similar project, Pazflor [8], Framo experienced excess of vibrations according to the acceptance criteria for the PB. This was caused by a peak in the response spectrum close to $0,5 \times n$. Their hypothesis was that the eigenfrequency of the PB was exited and they initiated a more extensive investigation regarding this matter. Their first conclusion was to add a support beam to increase the eigenfrequency and prevent the rocking mode, but nevertheless the problem continued to exist. After further investigation they discovered that the resonance was caused by the valve that is used to simulate resistance in the loop. It was mounted too close to the PB. By using another valve located further away the problem disappeared. This is a typical example illustrating that the problem is not always where it seems to be, and that thinking literally outside the box is crucial.

4.2.3 Material substitution

Another possibility that deserves some attention is substitution of materials. By replacing some of the metal with composite material one could decrease the vibrating mass (decrease the momentum) yet achieve the same stiffness. Since the system is isolated from the corrosive offshore environment by the enclosure, it does not have as high demands to material resistivity as usual for offshore equipment. Some specific cases should be compared by defining material indexes to study this option closer. For guidance the material index derived earlier, eq. 2.6, is used to state the obvious. Note that the material at the top of table 4.3, stainless steel (1.4404), is the material used for all parts in the module.

Tab. 4.3: Comparing materials with the material index method

Material	*Type*	*Youngs modulus* [Gpa]	*Density* [kg/m^3]	i
Stainless steel	1.4404	200	7980	0,025
Aluminium	Alloys, general	70	2700	0,026
Titanium	Alloys, general	107	4700	0,023
Composite	S Glass - Epoxy	52,2	1976	0,026
Composite	HM Carbon - Epoxy	211,8	1580	**0,134**

Although the material index used in table 4.3 is based on a cantilever beam loaded in the composites fibre direction, it is a good indicator. It is quite obvious that the Carbon/Epoxy is superior from a purely dynamic point of view. However, the price and the change in geometry (space requirements) are not taken into account here.

4.3 Results

Averaging the RMS velocity geometrically indicated that the HPU contributes the most to the RMS velocity of the skid, thus the vibrations emitted to the deck. This suspicion was confirmed by studying the response spectra, in addition to reveal that the HPU vibrations are disturbing the PB. Studying the mode shapes revealed that the HPU was altering the most at the critical frequencies.

To decrease the vibrations, mounting AVMs underneath the HPU seems to be the best solution. In addition, the use of active mass dampers on the skid should be considered since the load is highly dominated by harmonic loads at fixed frequencies. Semi-active dampers does not seem to be a feasible solution, but it could make an interesting research project in the future.

As far as I am concerned, installing additional supportive beams is not the best solution to limit the deck emitted vibrations since the response spectra are dominated by high frequency vibrations. The DE response spectra contains a lot of low frequency vibrations so if anything should be made stiffer, this would be my first suggestion to investigate.

I am convinced it is a good idea to discuss the use of composite materials, but this would require a lot of time. Decreasing the weight of the system by using composite material would clearly have more benefits than only dynamical ones. I will recommend the proposal for further research, but not as immediate action.

Only the creativity limits ideas of improvement; for example increasing the balancing grade or bearing quality are some ways of decreasing harmonic load. To limit my thesis, additional dampers is the solution I want to proceed with for the following analysis. This is also the suggestion I find most realistic.

5. ANALYSIS

5.1 Passive dampers

If passive dampers are installed underneath the HPU they would have to be stiff enough, so that the deflection of the HPU relatively to the engine does not exceed the alignment requirement demanded by the flexible coupling.

To determine which specific damper that should be used, a more detailed analysis needs to be performed. The analysis is normally performed by the AVM supplier[1], and requires more information about the equipment and its geometry in addition to information about the vessel it is placed on, the typical seaway conditions and the ambient climate.

Even though I do not have all of this information, I will still try to simulate the effect of the dampers and make a suggestion on AVM stiffness for the HPU.

This analysis requires finite element method, and a modal analysis is performed in Ansys. Since Ansys does not have a platform that matches my problem (other than transient analysis which would require days of solving), I was compelled to do some matrix algebra, post process and conclude utilizing MatLab.

5.1.1 The model

Stiffness

The diesel tank, HPU and PB are mounted directly on the skid with bolts. The stiffness of the bolts are calculated by $k = \frac{A_b E}{L}$ shown in table 5.1. The bolts are implemented in the model by springs of equivalent stiffness. This method is recommended by EDR and illustrated by the detail in figure 5.1.

Tab. 5.1: Bolt stiffness

	Dimension M	*Length* [mm]	*E* [MPa]	*Stiffness, k* [N/m]
HPU	16	60	200000	6,70E+08
PB	24	90	200000	1,01E+09
Fuel tank	16	60	200000	6,70E+08

[1] RubberDesign

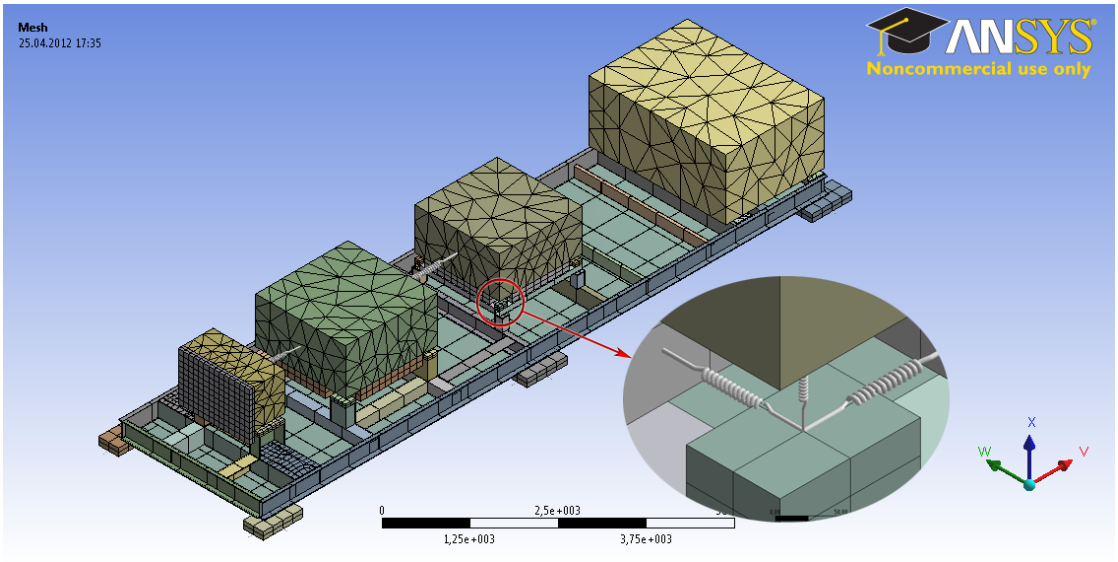

Fig. 5.1: The model used for FEM analysis

The stiffness of the deck, the AVMs underneath the DE and the flexi couplings are calculated by VibraTec and the respective suppliers, given in table 5.2. Note that the vertical stiffness of the AVMs, k_z, are slightly stiffer than estimated in section 1.3. This is because I was estimating the static stiffness from the documentation, while table 5.2 describes dynamic stiffness. These properties are also implemented in the model by springs as recommended.

Tab. 5.2: Given stiffness

	k_x [N/m]	k_y [N/m]	k_z [N/m]
Clov deck	5,00E+08	5,00E+08	2,00E+08
DE AVM	7,02E+07	7,02E+06	6,10E+06
Flexi couplings	8,82E+06	8,80E+04	8,80E+04

Moments of inertia and mass

Since a purely modal analysis is performed, and the global system behaviour rather than local deformation are the most interesting, the complicated geometry of the equipment is simplified to boxes (illustrated by figure 5.1). To make sure that these boxes behave like the real system they are defined with a massless material and a mass is added to each component in their real centroid (and not the centroid of the box). This enables control,

not only of the mass, but also of the moments of inertia. Calculation of moment of inertia is done by RubberDesign (for the DE), FRAMO (for the PB and HPU) and myself (for the enclosure). My calculations are simplified utilizing data from a finite element model used for lift calculation that FRAMO provided me with. From this model it was easy to extract the mass and centroid of all the components in the enclosure and further use the trivial formula for moment of inertia for a multi body part; $I = \sum_{i=1}^{N} m_i r_i^2$ in x–,y– and z-direction. My calculations are attached in appendix G.

5.1.2 The load

Linear behaviour is assumed and superposition applies since the system is solved modally. This assumption is essential for the rest of the analysis.

The load is unknown, but I do know that the PB, DE and HPU are the load generating equipment. In addition, I have response spectra for the vibration at these points gained from the FAT measurements, chapter 3. I generated FRFs[2] for vibration on the equipment regarding load on one piece of equipment at a time. This resulted in 9 response spectra, where the notation is described in table 5.3. Ansys had a limit on 3000 points on a FRF so to match the points from the measurements I created a function in MatLab, **interpolate.m** (appendix A), to interpolate between the points creating a FRF that matches the measured points exactly.

Tab. 5.3: FRF Descriptions

FRF	*Description*
PB-PB	Response of PB due to load on PB
PB-DE	Response of DE due to load on PB
PB-HPU	Response of HPU due to load on PB
DE-PB	Response of PB due to load on DE
DE-DE	Response of DE due to load on DE
DE-HPU	Response of HPU due to load on DE
HPU-PB	Response of PB due to load on HPU
HPU-DE	Response of DE due to load on HPU
HPU-HPU	Response of HPU due to load on HPU

I assembled these FRFs in diagonal matrices forming a giant sparse matrix (9603×9603) in MatLab and made an equation with the response versus the load. Since the response is known, this enabled me to get an estimate for the load. Equation 5.1 describes this

[2] Frequency Response Function

relationship.

$$\begin{bmatrix} \text{diag(PB-PB)} & \text{diag(DE-PB)} & \text{diag(HPU-PB)} \\ \text{diag(PB-DE)} & \text{diag(DE-DE)} & \text{diag(HPU-DE)} \\ \text{diag(PB-HPU)} & \text{diag(DE-HPU)} & \text{diag(HPU-HPU)} \end{bmatrix} \begin{bmatrix} F_{\text{PB}} \\ F_{\text{DE}} \\ F_{\text{HPU}} \end{bmatrix} = \begin{bmatrix} R_{\text{PB}} \\ R_{\text{DE}} \\ R_{\text{HPU}} \end{bmatrix} \tag{5.1}$$

Further, I generated yet three more FRFs describing the response of the middle support feet due to load on the PB, DE and HPU. Finally I used superposition to determine the response of the support feet, which describes the vibration emitted to the deck. All this is done in the script **Force.m** (appendix B) and the results from this script are plotted in figure 5.2, 5.3 and 5.4.

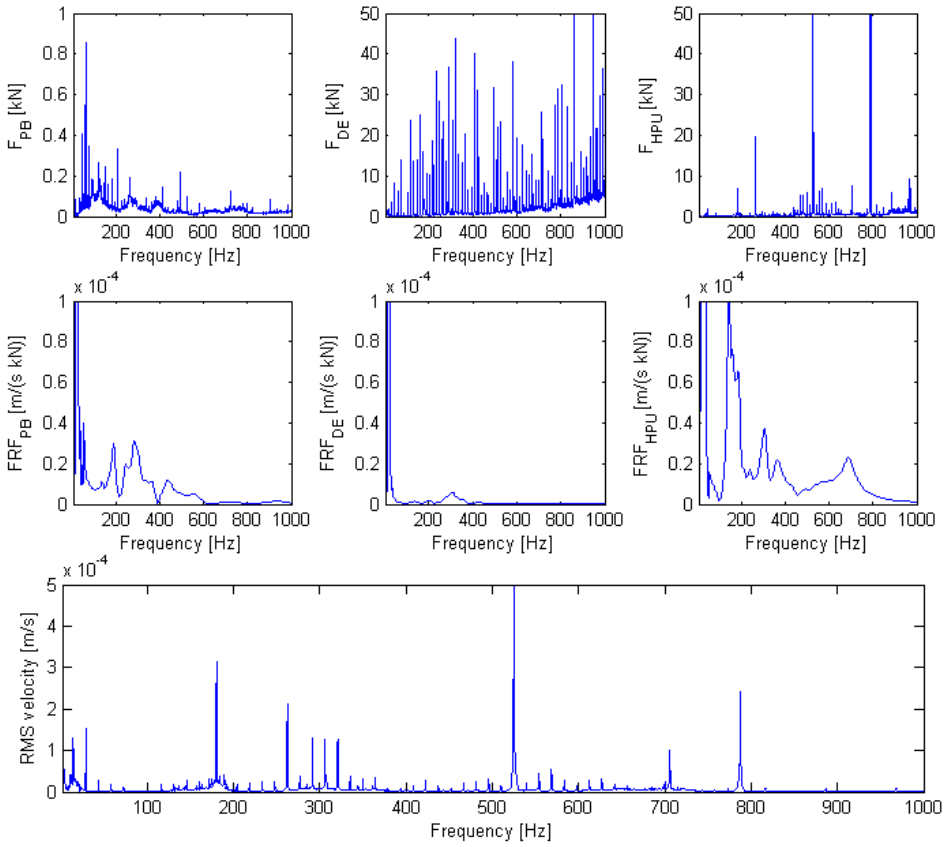

Fig. 5.2: Spectral analysis of the system

The upper three plots in figure 5.2 shows the loads calculated from equation 5.1, they will be kept constant throughout the following analysis.

The force generated by the PB, F_{PB}, is practically negligible compared to the other loads, this is reasonable because the PB is an impeller pump (all shafts and impellers are balanced) and has no reciprocating parts.

The DE load, F_{DE}, corresponds to the harmonics as described in section 2.2, and it also looks reliable. The fact that the load increases with the frequency is a bit odd and it is probably caused by inaccuracies in the FRFs at the high frequencies where the amplification is close to zero. However, these inaccuracies cancel out since the FRF describing support vibration due to F_{DE} is correspondingly low at the high frequencies. This is emphasized in figure 5.3.

The loads generated by the HPU, F_{HPU}, are small at the low frequencies and have three characteristic peaks at the piston frequency harmonics (multiples of 9 by the engine frequency), this is also in agreement with the theory described in section 4.1.2.

The three plots in the middle shows the FRF for the FWP module support point vibration due to the loads from the PB, DE and HPU respectively. The FRF regarding F_{DE} provides low amplification for high frequency load. This is because the DE is mounted on soft AVMs compared to the PB and HPU which are bolted directly on the skid.

Finally, the support response is plotted in the very bottom. It is obtained by utilizing superposition in the following way:

$$R_{Support} = F_{PB}FRF_{PB} + F_{DE}FRF_{DE} + F_{HPU}FRF_{HPU} \tag{5.2}$$

Figure 5.2 is made to visualize all the contributions in equation 5.2. The analysis will consist of studying how mounting AVMs underneath the HPU will influence the FRFs, thus the vibrations which are emitted to the deck.

Validating the model

To validate the model I compared the measured response of the module support from chapter 3 with the estimated response, figure 5.2. Both the estimated support response and the measured support response are plotted together in figure 5.3. This is a good verification because the support response is not used to estimate the load, thus the estimated loads and their interaction with the model are compared to real measurements of the system.

Although the model, figure 5.1, is pretty simple compared to real life, figure 3.1, the results are matching surprisingly good. They are definitely related and studying how damping will influence this simple model will clearly reflect how damping will influence the real system. The difference it RMS velocity is approximately 10%.

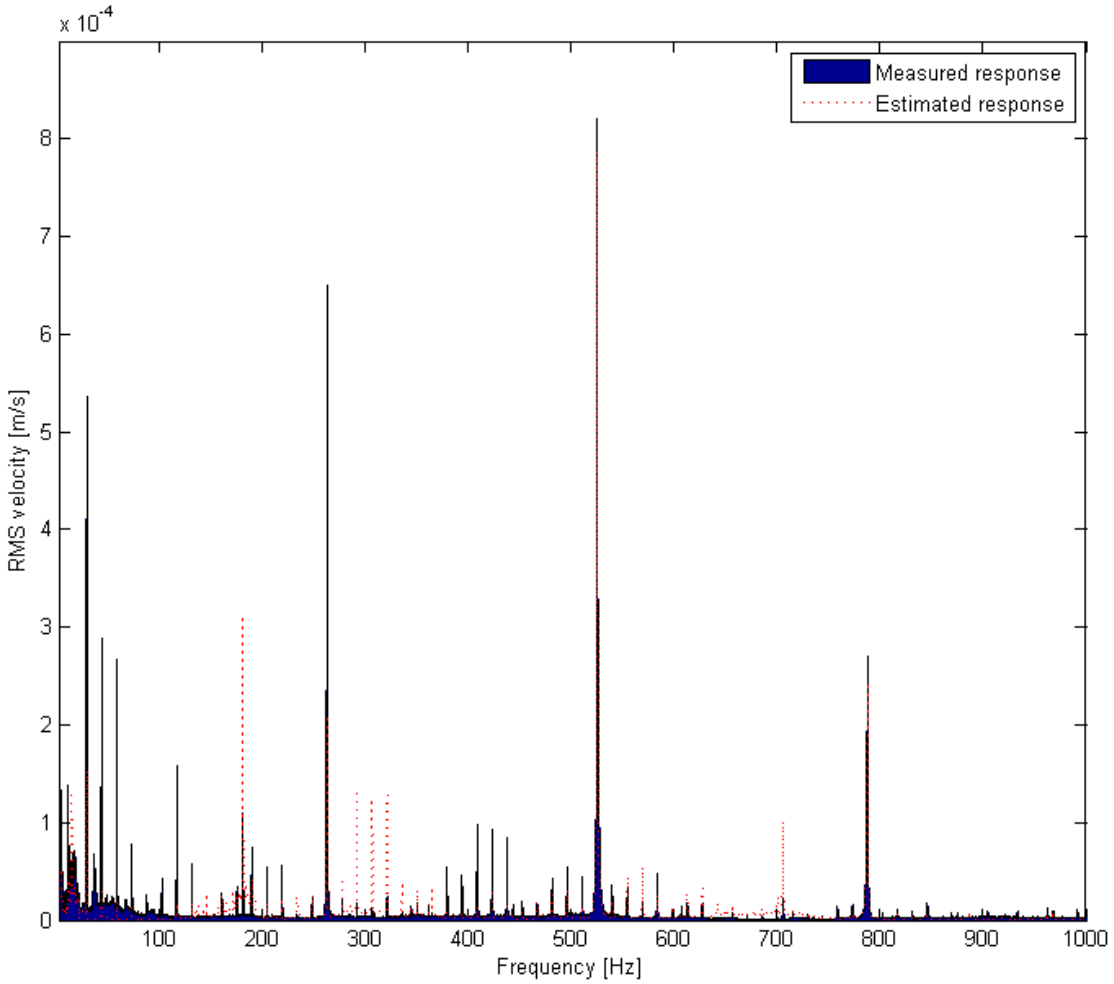

Fig. 5.3: Model verification

Estimating the potential

In figure 5.4 the terms in equation 5.2 corresponding to their respective equipment is coloured according to the legend. Table 5.4 illustrates that the PB does not contribute much to the deck emitted vibration, the HPU gives the dominating contribution with more than 70% of the RMS velocity. When it comes to low frequency vibration on the other hand, the DE is dominating in spite of the fact that it is mounted on AVMs. This is because, as earlier insinuated, a soft foundation is amplifying rather than suppressing low frequency vibrations. If the low frequency vibrations are the main concern, it is impossible to influence them much by mounting the HPU on AVMs. Figure 5.4 illustrates that something has to be done to the DE to limit the low frequency vibrations.

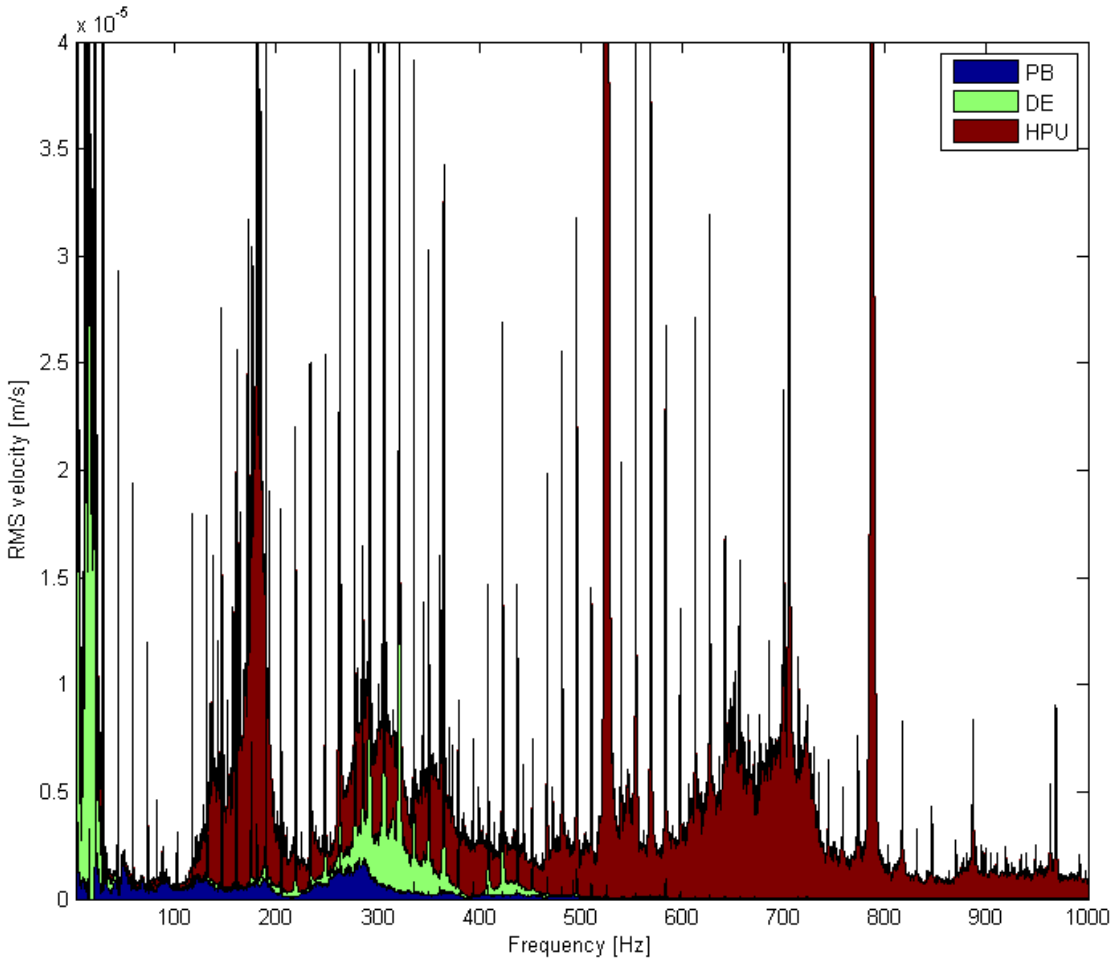

Fig. 5.4: Equipment contribution to deck emitted vibration

Tab. 5.4: Equipment contribution to deck vibration

	[2-1000]Hz		[2-100]Hz	
PB	0,033m/s	2,26 %	0,023m/s	4,60 %
DE	0,395m/s	26,96 %	0,322m/s	64,12 %
HPU	1,037m/s	70,78 %	0,157m/s	31,28 %
Total	1,465m/s	100,00 %	0,502m/s	100,00 %

5.1.3 Modelling the effect of AVMs on the HPU

To get a good picture of how damping of the HPU would influence the system, I studied three different cases in addition to the first case which is the system as it is;

Tab. 5.5: Case descriptions

Case #	*Foundation stiffness,* k_{HPU}	*Description*
Case 1	6,7E8 N/m	No damping, as it is now
Case 2	7E7 N/m	Stiff AVMs
Case 3	7E6 N/m	Almost the same AVMs as on the DE
Case 4	7E5 N/m	Very soft AVMs

In addition to plot the visualization of equation 5.2 (similar to figure 5.2) for every case, I have also calculated three factors;

- The RMS velocity ratio for [2-1000]Hz

  This is the full spectrum RMS velocity of the current case divided by case 1, used to visualize the change of vibration energy.

- The RMS velocity ratio for [2-100]Hz

  This is the RMS velocity at the low frequencies (up to 100 Hz) of the current case divided by case 1, used to visualize the change of low frequency vibration energy.

- The guiding misalignment

  Six new FRFs for every case are generated. They describe the motion of the shaft point on the HPU and DE due to load on the different equipment. They are then multiplied with the load. For a worst case conservative measure they are added together in a final superposition. This is a conservative measure because the displacement is relative to the ground (and not to the skid), so the motion of the skid is causing excessive relative motion between the HPU and DE twice. The forces in x– and z-direction would also influence the real misalignment, so the measure is only used for guidance. Rather than evaluating the actual magnitude of the misalignment, the trend is evaluated. The measure is a good indicator for when the HPU foundation becomes too soft.

All FRFs are generated with Ansys and evaluated with **Plot_variable_k.m** and **Displacements.m** (appendix C and D).

The RMS velocity ratios of case 1 is of course 100 % and the guiding misalignment is: 0,189°.

Case 2: $k_{HPU} = 7E7N/m$

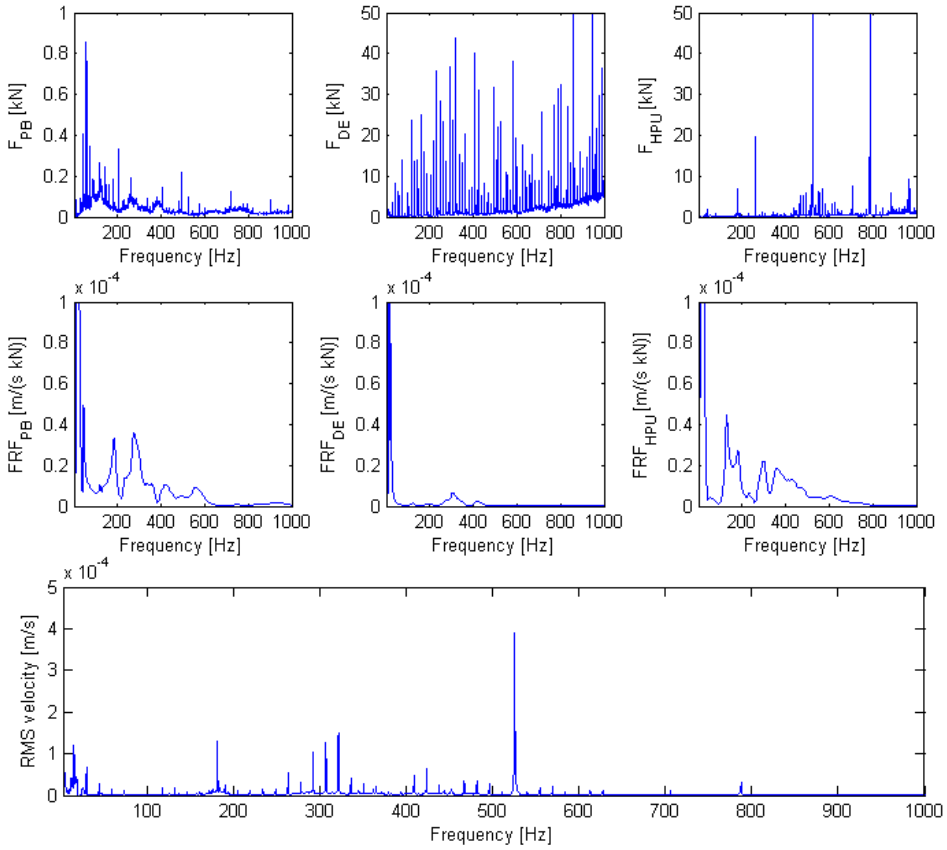

Fig. 5.5: Case 2: Visualization of equation 5.2

Comparing figure 5.5 to figure 5.2 shows that making the foundation softer damps the peaks of $\mathrm{FRF}_{\mathrm{HPU}}$, in addition to decreasing the eigenfrequencies (shifting the peaks to the left). This mainly results in reducing the final high frequency vibration.

The RMS velocity ratio for [2-1000]Hz is:	$57,3\%$
The RMS velocity ratio for [2-100]Hz is:	$94,0\%$
The guiding misalignment:	$0,193°$

Case 3: $k_{HPU} = 7E6N/m$

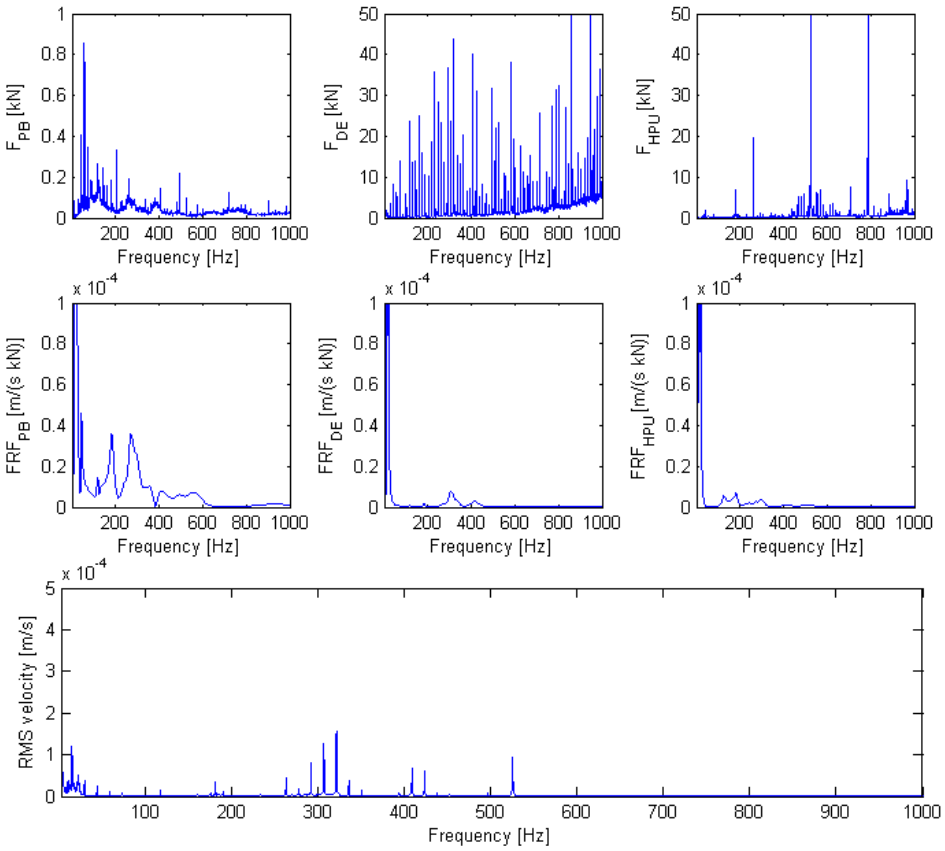

Fig. 5.6: Case 3: Visualization of equation 5.2

Reducing the foundation stiffness even more is almost eliminating the high frequency vibrations caused by the HPU and the eigenfrequencies are decreased farther. This results in a greater decrease of the overall vibration, but a slight increase in the low frequency vibration. Note that $\mathrm{FRF_{HPU}}$ is similar to $\mathrm{FRF_{DE}}$, this is because the AVMs in this case are almost the same for the HPU and the DE.

The RMS velocity ratio for [2-1000]Hz is:	$40,8\%$
The RMS velocity ratio for [2-100]Hz is:	$96,2\%$
The guiding misalignment:	$0,207°$

Case 4: $k_{HPU} = 7E5N/m$

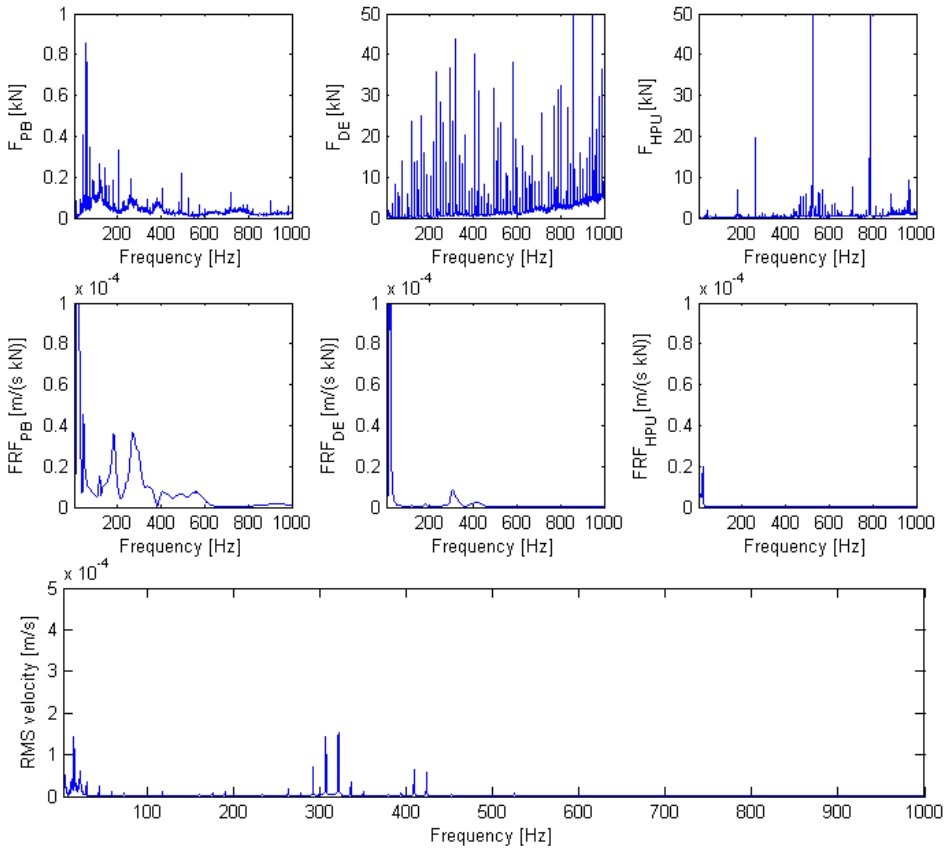

Fig. 5.7: Case 4: Visualization of equation 5.2

In the softest foundation case, the HPU is getting close to unstable. This is because all the eigenfrequencies are squeezed in the lowest part of the spectrum. The low frequency vibrations are amplified causing an increase in both the RMS velocity ratios. A more serious issue is that the soft foundation allows the HPU to drift exceptionally more than in the other cases and the misalignment gets close to fatal.

The RMS velocity ratio for [2-1000]Hz is:	$43,6\%$
The RMS velocity ratio for [2-100]Hz is:	$112,5\%$
The conservative misalignment:	$1,110°$

5.1.4 Sensitivity analysis of the constant damping ratio

CDR is the simplest way of specifying damping ratio of a structure in Ansys. It is the method preferred by FRAMO and EDR in this type of analysis. CDR represents the ratio of actual damping to critical damping and FRAMO is traditionally using 4%. Structural damping is one of the biggest elements of uncertainty in a dynamic FEM analysis and EDR encouraged me to do a simple sensitivity analysis regarding this matter.

I generated FRFs in two different cases equivalent to case 1, only varying the CDR, to understand how the CDR influences the solution. The eigenfrequencies are visualized by the x-values [Hz] corresponding to the peaks in the FRFs. The eigenvalues are practically unchanged by small variations in the CDR, but the corresponding peaks get lower as the CDR increases. The FRFs are smoothed out causing higher amplification between the peaks when the CDR increases. This is illustrated in figure 5.8. The total visualization of equation 5.2, figure E.1, is attached together with the script used to make it in appendix E.

I calculated the RMS velocity ratio in the same way as earlier to generalize the trend, this is illustrated in figure 5.9. The response decreases rapidly as the CDR increases. An interesting observation is that the low frequency response seems to be less sensitive to the CDR, this is also visible in figure E.1.

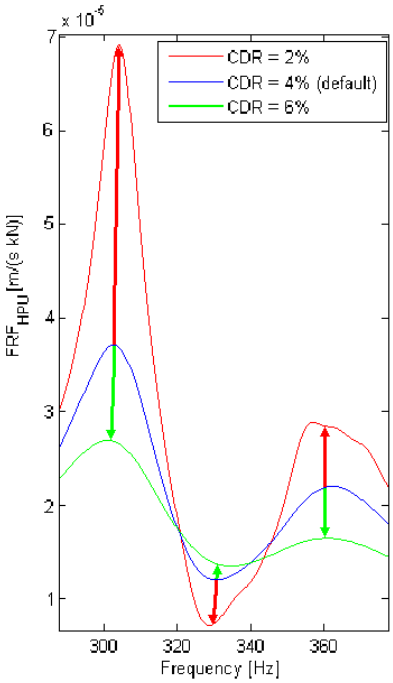

Fig. 5.8: CDR sensitivity

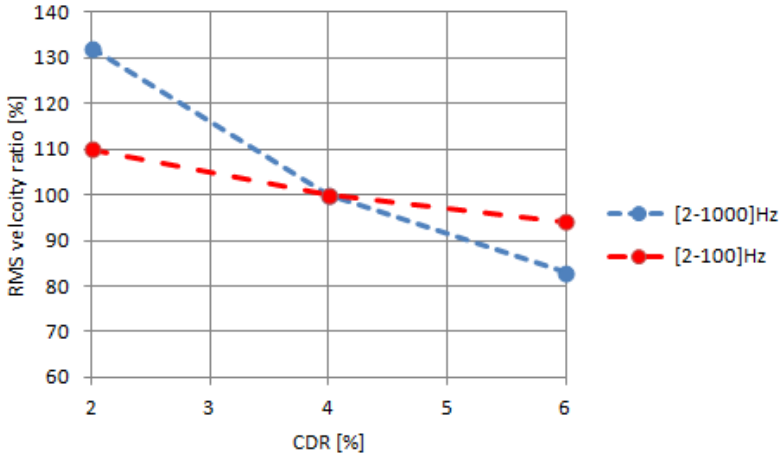

Fig. 5.9: RMS velocity ratio as a function of CDR

5.1.5 Results

The eigenmodes

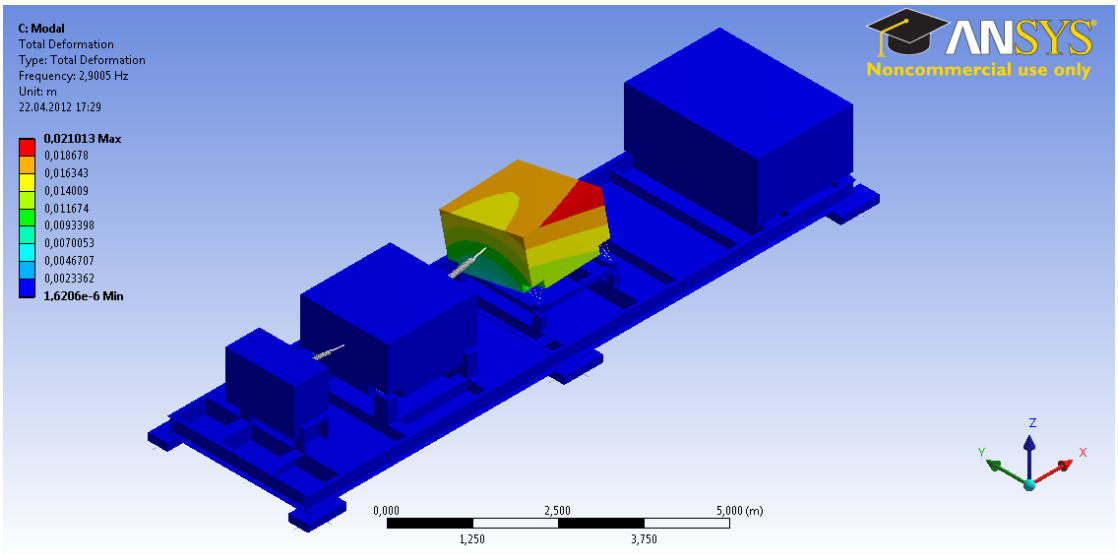

Fig. 5.10: HPU roll mode (rotation about the x-axis)

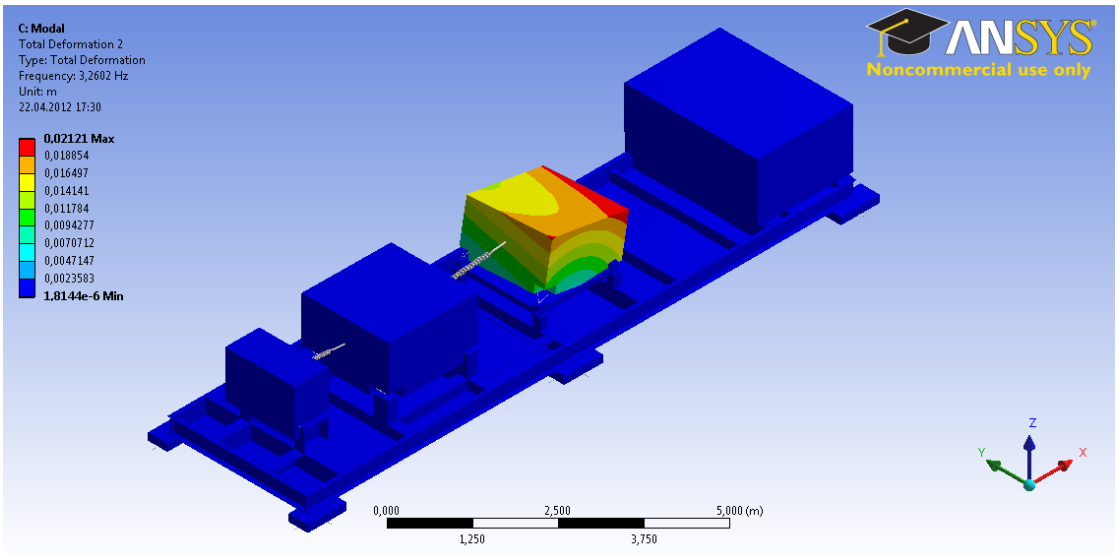

Fig. 5.11: HPU pitch mode (rotation about the y-axis)

It is important that the eigenmodes are appearing at "safe" frequencies. For instance since the engine is running with 29,2 Hz, this frequency would be a bad eigenfrequency to have in the system. As derived in section 2.2, multiples of this frequency should be avoided. A damped system provides low amplification for high frequencies, so extra attention is paid to the low frequency modes (below 100 Hz). Most modes are not affected by damping the HPU, but the two modes illustrated in figure 5.10 and 5.11 are decreasing rapidly as the foundation stiffness decreases. An interesting observation is that the eigenfrequency corresponding to the roll mode of the HPU, figure 5.10, originally was close to the main frequency, 29,2 Hz. Figure 5.12 illustrates the motion of these eigenfrequencies as the foundation gets softer. As mentioned earlier the system typically gets unstable when the eigenfrequencies approaches zero.

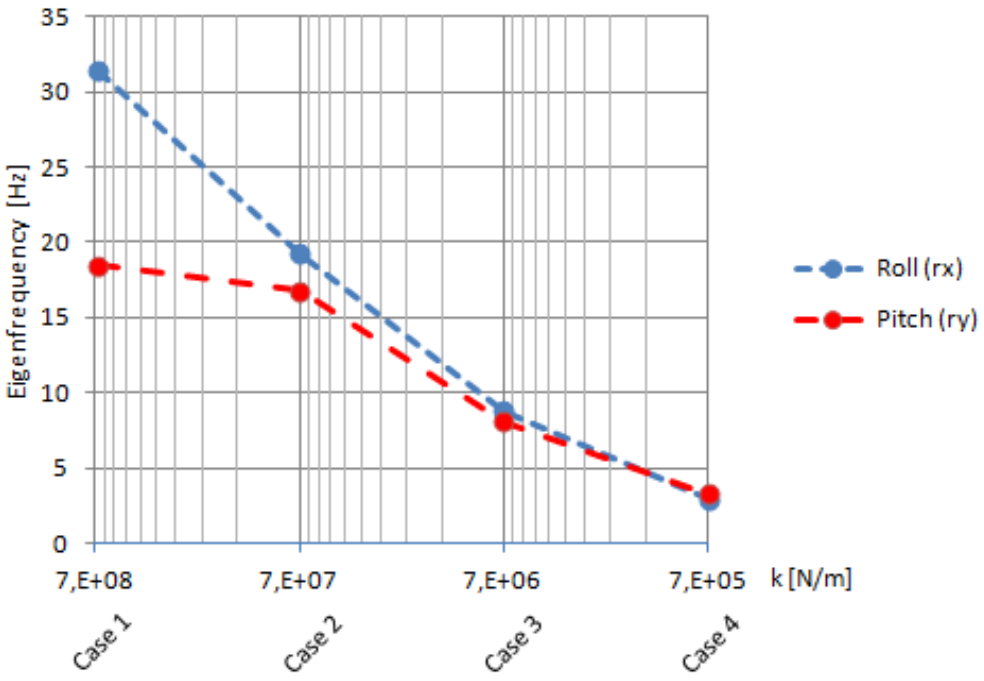

Fig. 5.12: Eigenfrequencies versus HPU foundation stiffness

Figure 5.12 shows that both case 1 and case 2 have an eigenfrequency which is approximately 2,2 Hz away from a fundamental frequency. The closer a load gets to an eigenfrequency, the more vibration it will cause.

Case 1:	H1 and HPU roll mode	$31,4\text{Hz} - 29,2\text{Hz} = 2,2\text{Hz}$
Case 2:	0,5H1 and HPU pitch mode	$\frac{31,4\text{Hz}}{2} - 16,8\text{Hz} = 2,2\text{Hz}$

It has also been shown that case 4 is getting close to unstable.

Vibration and misalignment

To summarize the case studies the values calculated in each case are plotted against the foundation stiffness in figure 5.13. The interesting trend is already discussed and it is illustrated in figure 5.13.

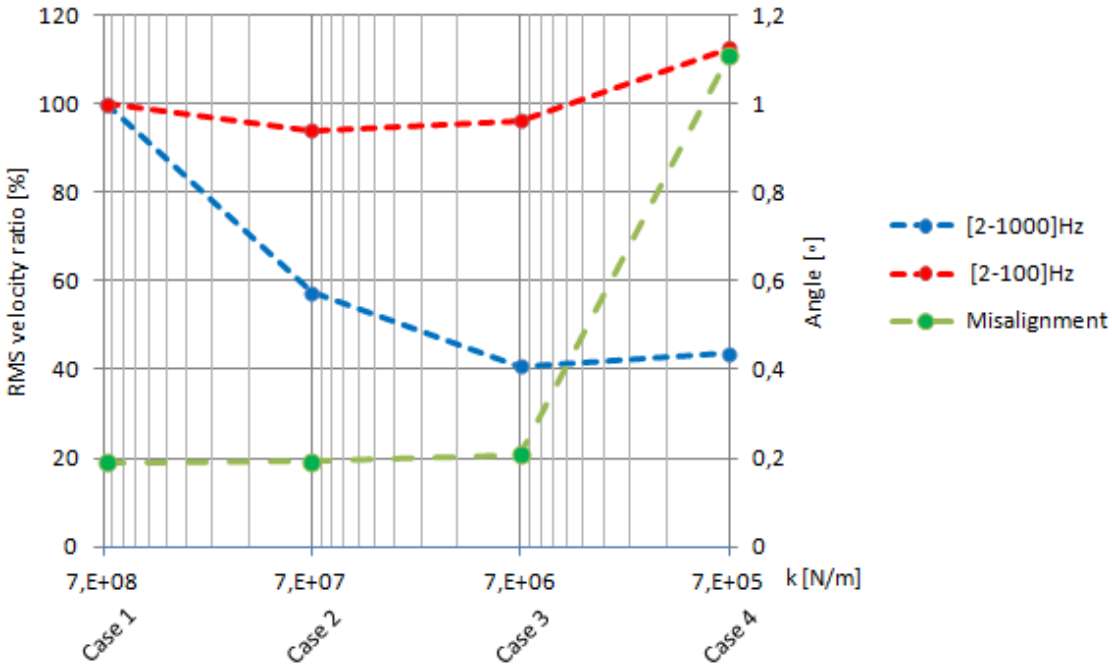

Fig. 5.13: RMS velocity ratio and misalignment versus HPU foundation stiffness

Figure 5.13 shows that as the HPU foundation gets softer the vibration decays. The high frequency vibration is damped the most since the eigenfrequencies decrease. When the foundation gets too soft on the other hand, the vibrations grow and the low frequency vibrations get worse than in the undamped case. The most significant issue is how the misalignment shoots up when the foundation gets to soft.

As seen from figure 5.4 and table 5.4 the DE is the biggest contribution to low frequency vibration and damping of the HPU can not influence this much. The optimal choice of HPU foundation stiffness is probably not any of the round values studied here, it is more likely somewhere in between case 2 and case 3. Either way, damping of the HPU within limits only seems to have good outcomes regarding vibration limitation.

The CDR sensitivity analysis confirms that damping influences the high frequency vibration farther than the low frequency vibrations. Since the eigenvalues are not affected much by the damping it can also be concluded with that the trends of the results are valid regardless of the CDR, while the quantitative results are dependent of the CDR.

5.2 Active mass dampers

Most literature about AMD is regarding structures and civil engineering. It was not easy to find an AMD solution that was directly applicable to this case. However, to understand the concept better in practice I read a research paper about tuned mass damping of railway tracks in Hong Kong, from a collection of technical reports released by Springer [13]. The trains have a size that is comparable to the FWP module, and the paper inspired me to the thought of mounting similar AMDs on the skid, equivalent to how these AMDs are mounted to the railway. This is obviously not an "on the shelf" product, it has to be designed specifically for a particular track, matching the spectrum by being tuned to the frequency associated with the peak vibration velocity.

(a) Schematic diagram (b) Real installation

Fig. 5.14: Active mass dampers on railroad tracks

The concept is illustrated on figure 5.14(a). Firstly, the energy of movement is absorbed by the elastomer material, but more importantly the rail vibration causes the masses to oscillate. The idea is to control these oscillations in such a way that they generate a counterforce that cancels out vibration at a certain frequency. The elastomer works as a spring and by varying the material properties one can tune the oscillation to specific frequencies. To make a proposal for an equivalent damper design for the FWP module skid, the following needs to be studied:

- The shape and fixing constraints

  Where on the skid should the damper be mounted?

  How should the damper be mounted to the skid?

  How much clearance do we have?

- Internal arrangement to give effective vibration reduction (steel size ad spacing)

  Which frequencies do we wish to cancel out?

  What is the magnitude of the vibrations?

  How much mass is associated with the vibration?

Which materials should we use for the damper?

What is the material properties of the materials used?

When this is determined a comprehensive finite element method analysis should be carried out, optimizing the design with parameter variables. This job is a master thesis, possibly a Ph.D., by itself and will not be attempted in this thesis. Still a principal quick calculation will be carried out just to accentuate the idea.

I will investigate the effect of a TMD in one direction only, considering the whole skid as one massive body subjected to harmonic load in the respective direction. The following data is needed to perform this analysis:

- The mass of the system

  $m = 59500\text{kg}$

- The stiffness of the deck

  Given in table 5.2; $k/2 = 5000\text{MN/m}$

- The response

  Available from the measurements in section 3.

First I will make simple models using parameters for the properties of the TMD.

Secondly I will convert the response to time domain and utilize the result and a simple model to estimate the load on the system.

Then I will implement the TMD and study how the different parameters affect the system and optimize it by varying these parameters.

Finally I will study the implementation of an actuator on the TMD.

5.2.1 Simplifying the model

The system becomes as illustrated in figure 5.15(a) by considering only transversal vibration (y-direction) and modelling the whole skid as one rigid part. The implementation of a TMD working solely in this direction could then be modelled by an additional mass attached to the original mass with spring and damper as illustrated in figure 5.15(b).

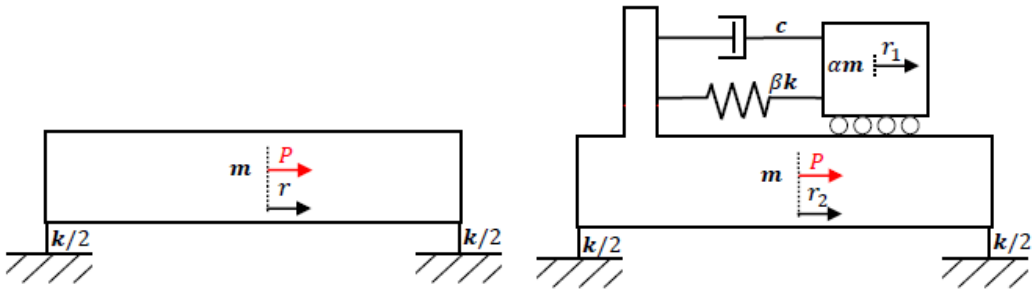

(a) Model 1: The skid alone (b) Model 2: The skid with a TMD

Fig. 5.15: Simplified models

Model 1: The skid alone

The model illustrated in figure 5.15(a) is the easiest dynamic system possible. Although the theory is assumed known and the system is trivial, a quick recap will be given:

Eigenfreqency: $$f_n^2 = \frac{k}{4\pi^2 m}$$

Frequency ratio: $$\beta = \frac{\overline{f}}{f_n} \tag{5.3}$$

The response amplitude if P is harmonic: $$r = \frac{P}{k\,|1-\beta^2|}$$

The velocity response amplitude: $$\dot{r} = \frac{2\pi\overline{f}}{k\,|1-\beta^2|} \cdot P \tag{5.4}$$

The load amplitude if the velocity response is known: $$P = \frac{rk\,|1-\beta^2|}{2\pi\overline{f}} \tag{5.5}$$

Equation 5.5 is the only formula needed to estimate the forces on the system that generates the response measured.

Model 2: The skid with a TMD

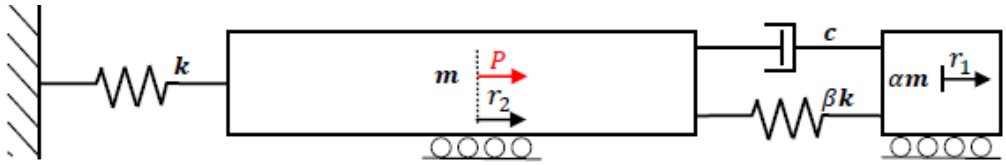

Fig. 5.16: Classical SMD diagram equivalent to model 2

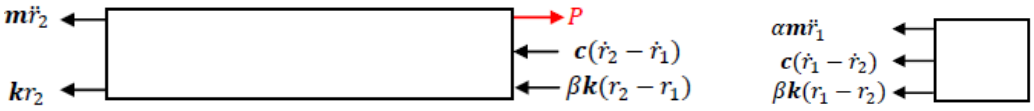

(a) The skid (b) The TMD

Fig. 5.17: Free body diagrams

From figure 5.17(a) and 5.17(b) it is quite easy to set up the equilibrium equations and assemble the property matrices:

Eq'm of element 1, the TMD $\alpha m\ddot{r}_1 + c\dot{r}_1 + \beta k r_1 - c\dot{r}_2 - \beta k r_2 = 0$ (5.6)

Eq'm of element 2, the skid $m\ddot{r}_2 + c\dot{r}_2 + k(1+\beta)r_2 c\dot{r}_1 - \beta k r_1 = P$ (5.7)

Choosing: $\mathbf{r} = \begin{bmatrix} r_1 & r_2 \end{bmatrix}^T$

Results in the mass matrix: $\mathbf{M} = m \begin{bmatrix} \alpha & 0 \\ 0 & 1 \end{bmatrix}$

The damping matrix: $\mathbf{C} = c \begin{bmatrix} 1 & -1 \\ -1 & 1 \end{bmatrix}$

The stifness matrix: $\mathbf{K} = k \begin{bmatrix} \beta & -\beta \\ -\beta & 1+\beta \end{bmatrix}$

And the load vector: $\mathbf{P} = \begin{bmatrix} 0 \\ P \end{bmatrix}^T$

Such that: $\mathbf{M}\ddot{\mathbf{r}} + \mathbf{C}\dot{\mathbf{r}} + \mathbf{K}\mathbf{r} = \mathbf{P}$

The undamped eigenfrequencies can be calculated from these property matrices by evaluating: $\det\left|\mathbf{K} - \frac{f_n^2}{4\pi^2}\mathbf{M}\right| = 0$:

$$f_1^2 = \frac{k}{8\pi^2 m}\left(\frac{\alpha+\beta+\alpha\beta - \sqrt{\alpha^2\beta^2 + 2\alpha^2\beta + 2\alpha\beta^2 + (\alpha-\beta)^2}}{\alpha}\right) \tag{5.8}$$

$$f_2^2 = \frac{k}{8\pi^2 m}\left(\frac{\alpha+\beta+\alpha\beta + \sqrt{\alpha^2\beta^2 + 2\alpha^2\beta + 2\alpha\beta^2 + (\alpha-\beta)^2}}{\alpha}\right) \tag{5.9}$$

L'Hôpitals rule quickly shows that both eigenfrequencies converges too the eigenfrequency in model 1 when α approaches 0. This is obvious because $\alpha = 0$ is equivalent to no TMD, hence both models become identical. This system can not be solved modally (because of $\mathbf{C}$), but since it is a small system it can be done analytically by using Fourier transformation. The theory is assumed known and derived in my previous paper [14]. A quick derivation will still be performed:

FT of eq. 5.6
$$\hat{r}_1\left[(2\pi \mathrm{i}\overline{f})^2\alpha m + (2\pi \mathrm{i}\overline{f})c + \beta k\right] - \hat{r}_2\left[(2\pi \mathrm{i}\overline{f})c + \beta k\right] = 0$$

Hence:
$$\hat{r}_1 = \frac{(2\pi \mathrm{i}\overline{f})c + \beta k}{-4\pi^2\overline{f}^2\alpha m + (2\pi \mathrm{i}\overline{f})c + \beta k}\hat{r}_2 \tag{5.10}$$

FT of eq. 5.7
$$\hat{r}_2\left[(2\pi \mathrm{i}\overline{f})^2 m + (2\pi \mathrm{i}\overline{f})c + (1+\beta)k\right] - \hat{r}_1\left[(2\pi \mathrm{i}\overline{f})c + \beta k\right] = \hat{P}$$

Inserting eq 5.10
$$\hat{r}_2\left[(2\pi \mathrm{i}\overline{f})^2 m + (2\pi \mathrm{i}\overline{f})c + (1+\beta)k - \frac{\left((2\pi \mathrm{i}\overline{f})c + \beta k\right)^2}{-4\pi^2\overline{f}^2\alpha m + (2\pi \mathrm{i}\overline{f})c + \beta k}\right] = \hat{P}$$

Rearranging:
$$\hat{r}_2\left[k\left(1 - \frac{4\pi^2\overline{f}^2 m}{k}(1+\alpha) - \frac{\left(\alpha\frac{4\pi^2\overline{f}^2 m}{k}\right)^2}{\beta + \frac{2\pi \mathrm{i}\overline{f}c}{k} - \alpha\frac{4\pi^2\overline{f}^2 m}{k}}\right)\right] = \hat{P} \tag{5.11}$$

Defining:
$$B^2 = \frac{4\pi^2\overline{f}^2 m}{k} \tag{5.12}$$

Eq 5.11 and 5.12 gives:
$$\hat{r}_2 = \left[k\left(1 - B^2(1+\alpha) - \frac{(\alpha B^2)^2}{\beta + \frac{2\pi \mathrm{i}\overline{f}c}{k} - \alpha B^2}\right)\right]^{-1}\hat{P} \tag{5.13}$$

Note that the B defined in equation 5.12 is equivalent to the frequency ratio in model 1, equation 5.3. The reason it is not referred to as β here is because it is not the frequency ratio (unless $\alpha = 0$) and I do not want to confuse it with the stiffness constant, β, which is used in this model. Again, if the loading is harmonic it is easy to transform equation 5.13 back to time space. The amplitude of the velocity response of the skid due to harmonic load becomes:

$$\dot{r}_2 = \frac{2\pi\overline{f}}{k\left|1 - B^2(1+\alpha) - \frac{(\alpha B^2)^2}{\beta + \frac{2\pi \mathrm{i}\overline{f}c}{k} - \alpha B^2}\right|} \cdot P \tag{5.14}$$

Note that if $\alpha = 0$, equation 5.14 simplifies to equation 5.4. This is obvious because when $\alpha = 0$ the models become identical as stated earlier.

5.2.2 The load

Converting to time domain

The first step to get the load is to convert the response to time domain. This is done by using a method described by Strømmen [15]. The method is good and not too comprehensive in this case, since the response is dominated by six narrow-banded peaks. The method implies to calculating the area under each peak which represents the amplitude of the harmonic response at the respective frequency. I generated an auto-spectrum with Pulse LabShop, figure 5.18. The numbers on the figures indicate the peak number which is referred to in table 5.6.

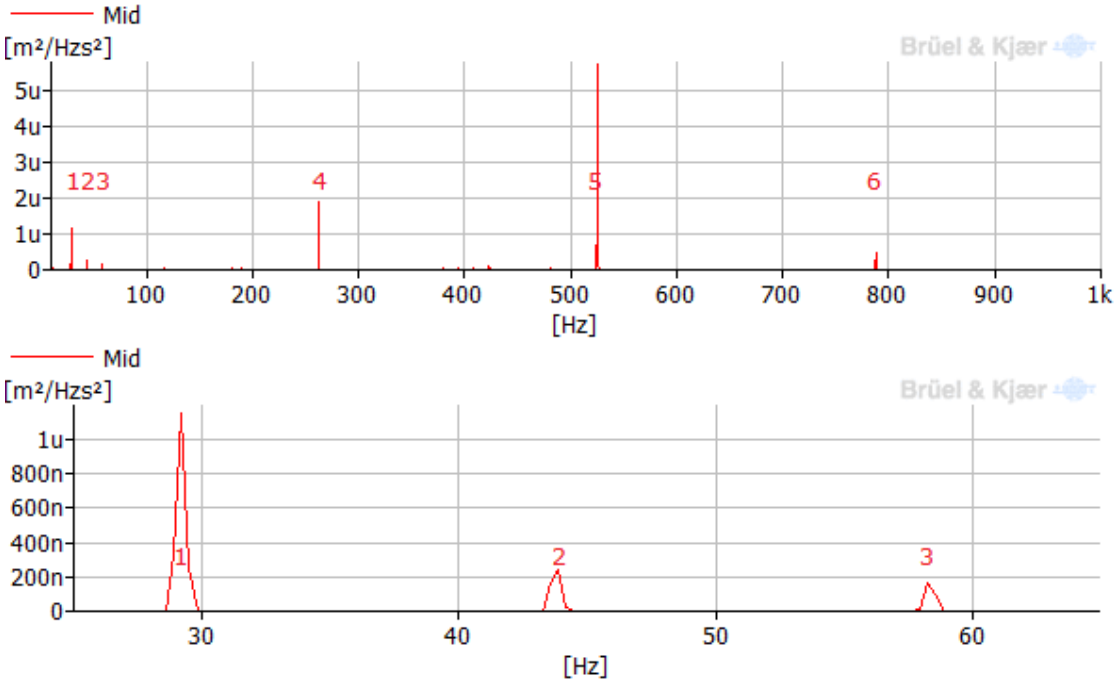

Fig. 5.18: Auto-spectral density of mid support response, S.

I extracted the exact values of the peaks (see table 5.6) from Pulse LabShop, and the areas are calculated by assuming that the spectrum have an isosceles triangle around each peak. Figure 5.18 confirms this assumption. This gives the following formula for the velocity amplitudes;

$$c_k = \sqrt{S(f_k)\Delta f} \tag{5.15}$$

There is a slight difference compared to Stømmen's method since he used rectangles to determine the area.

The value, c_k, is the amplitude of the vibration velocity at the respective frequency. From eq. 5.15 and figure 5.18 I developed the following table:

Tab. 5.6: Calculating the load contributions

k #	$S(f_k)$ [m^2/Hz s^2]	f_k [Hz]	Δf [Hz]	c_k [m/s]
1	1,15E-06	29,17	0,94	1,04E-03
2	2,39E-07	43,75	0,94	4,74E-04
3	1,64E-07	58,33	0,94	3,93E-04
4	1,91E-06	262,50	0,94	1,34E-03
5	5,74E-06	525,00	0,94	2,32E-03
6	4,60E-07	787,50	0,94	6,58E-04

The superposition of these six waves makes up the total response. I simulated the response in excel, see figure 5.20. In the final superposition I introduced a small random phase delay between the engine response and the HPU pistons (since the engine is damped), I typically got values just around 2mm/s, which is quite close to the measured level of 1,9 mm/s (calculated in table 4.1), therefore it seems to be a reasonable approximation.

Another way of validating the results is to compare the peak response spectrum to the estimated result. This is different than the RMS spectrum for the support points, figure 4.6 and table 4.2. It turns out that the peak values, c_k, are practically exactly a factor of $\sqrt{2}$ greater then the RMS values in table 5.6. This confirms that the response is sinusoidal, and it is also consistent with the theory. To visualize this I also made a peak response spectrum for the mid support points, figure 5.19. In addition I made a peak response – and load spectrum from the numerical values with bars representing infinitesimally narrow-banded peaks at the significant frequencies, figure 5.21. These two figures match perfectly as well. These results indicate that the response is converted to time space successfully.

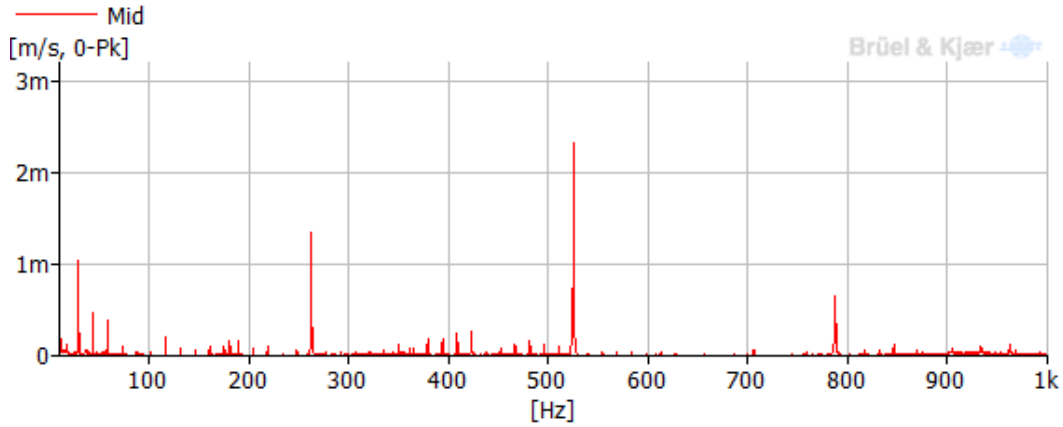

Fig. 5.19: Peak response spectrum of the mid support points

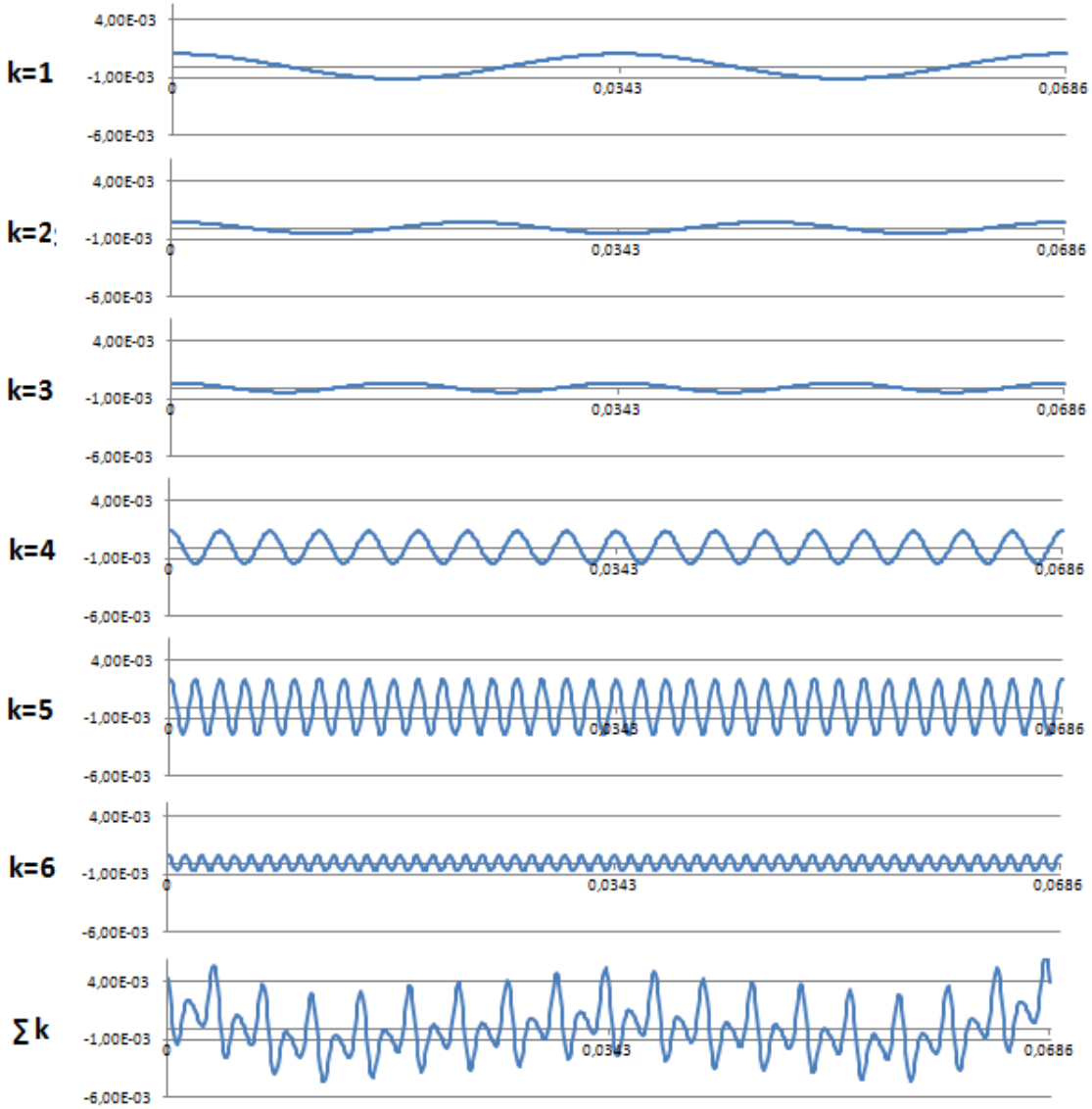

Fig. 5.20: Time simulation of the mid support response

Calculating the load

It is assumed that the measured response is the response of model 1, figure 5.15(a), subjected to purely harmonic loading. This assumption introduces a big uncertainty associated with the model simplification. The different loads with the significant frequencies are then easily found by utilizing equation 5.5. This resulted in table 5.7, where P_k represents the amplitude of the load at the respective frequency. The results are visualized in figure 5.21.

Tab. 5.7: Estimating the load

k #	f_k [Hz]	c_k [m/s]	β_k [rad/s]	P_k [N]
1	29,17	1,04E-03	4,47E-02	5,67E+06
2	43,75	4,74E-04	6,71E-02	1,72E+06
3	58,33	3,93E-04	8,94E-02	1,06E+06
4	262,50	1,34E-03	4,02E-01	6,80E+05
5	525,00	2,32E-03	8,05E-01	2,48E+05
6	787,50	6,58E-04	1,21E+00	6,07E+04

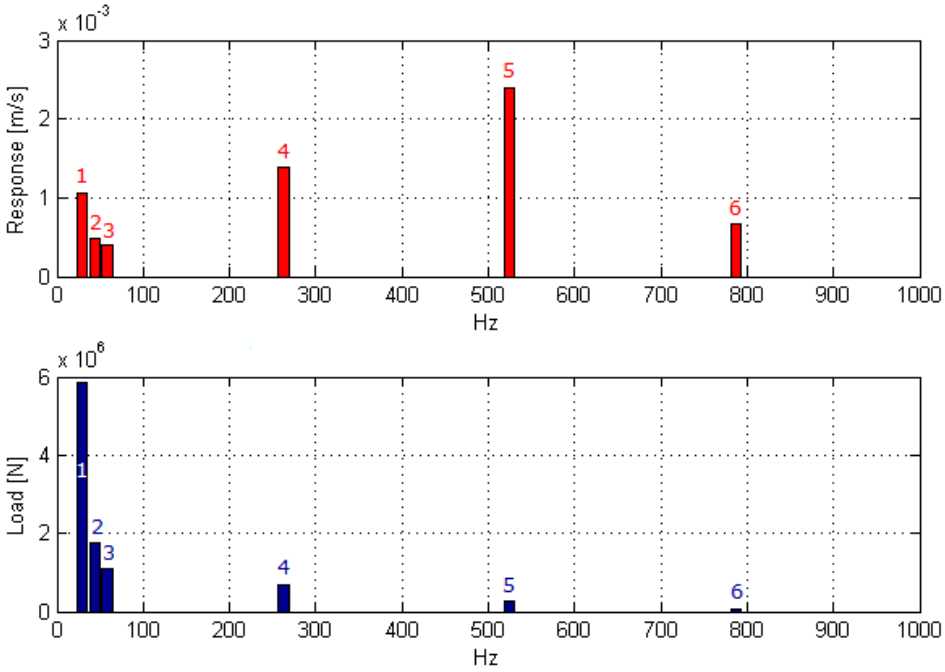

Fig. 5.21: The calculated response and load visualized with MatLab

5.2.3 Modeling the effect of the TMD

The load subjected to model 1 is now the same load which is subjected to model 2, figure 5.15(b). If $\alpha \neq 0$ then the response will be different. The response of the skid is the only response of interest, and it is given by equation 5.14.

This response is implemented in a MatLab function (appendix F), iterated through a for-loop creating an amplification function represented by the blue graph in the GUI.

The load, represented by the blue bars in the GUI, is then multiplied with the amplification. The product is the peak velocity response of the skid represented by the red bars in the GUI.

I turned these relations in to a MatLab GUI (appendix G) to visualize how the different parameters affect the amplification, and to easier tailor it to minimize the response. A guiding RMS ratio is also calculated to estimate the effect of the TMD.

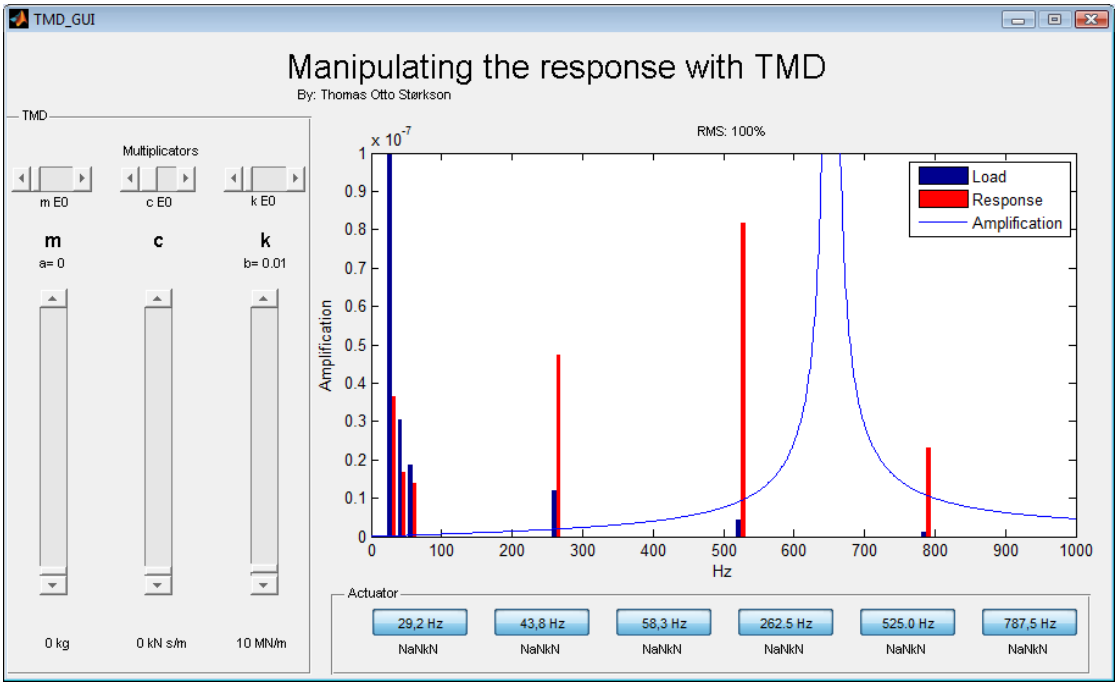

Fig. 5.22: MatLab GUI, initial configuration

In figure 5.22 I have chosen $\alpha = 0$ this is equivalent to no TMD, hence when both models coincide. The TMD ratio is 100% which indicates no RMS reduction, which is obvious. Note that the load and response (blue– and red bars) are scaled to fit the plot and have no relationship with the y-axis, they are only there to visualize the magnitudes.

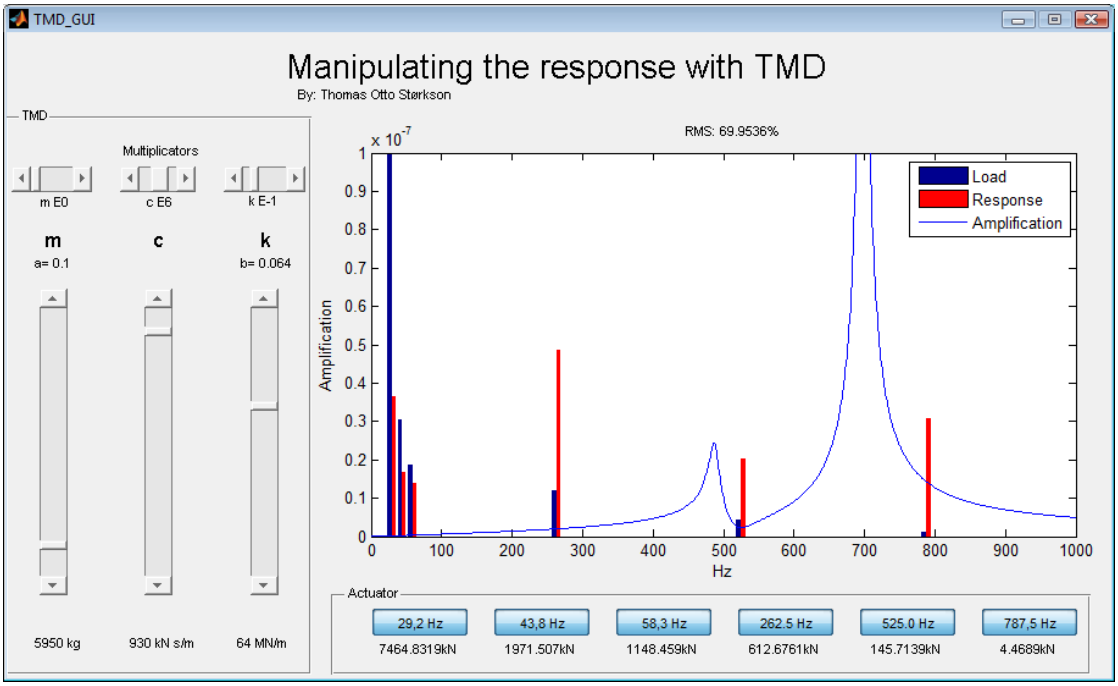

Fig. 5.23: MatLab GUI, with TMD

In figure 5.23 I have chosen $\alpha = 0.1, \beta = 0,064$ and $c = 930$kN s/m. This results in an RMS reduction by 30%

This is of course a very simplified model and a more comprehensive model would allow influencing more eigenvalues, resulting in a more efficient configuration of the TMD.

5.2.4 Implementation of an actuator

A more sophisticated active damper is the TMD with actuator. The idea is to cancel out the load at one of the significant frequencies.

An actuator is not used on the rail-track dampers mentioned earlier, and it may introduce more complications than benefits. Still, since the load appears at constant frequencies, I will take a quick look and see how beneficial it could be in this case. Model 3, figure 5.24, shows how an actuator could be implemented.

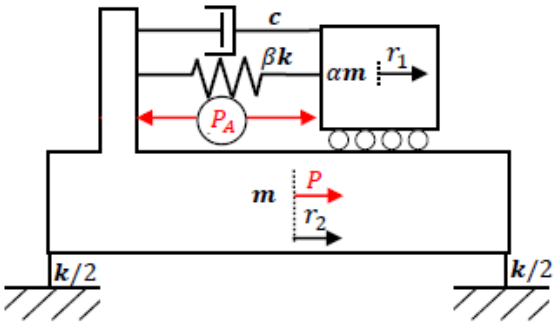

Fig. 5.24: Model 3: The skid with TMD and actuator

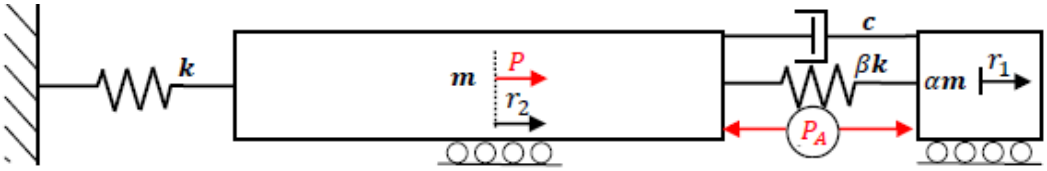

Fig. 5.25: Classical SMD diagram equivalent to model 3

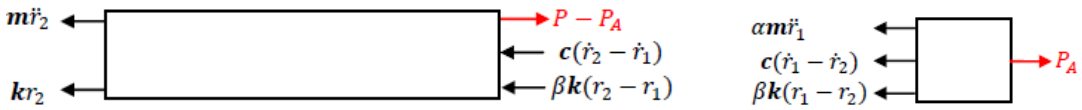

(a) The skid (b) The TMD

Fig. 5.26: Free body diagrams with actuator

From the free body diagrams, figure 5.26(b) and 5.26(a) it is obvious that the equations of motion are almost identical as before. All the property matrices are identical, but the load vector is different. Obviously the undamped eigenfrequencies and the amplification function remains the same.

Eq'm of element 1, the TMD $\alpha m\ddot{r}_1 + c\dot{r}_1 + \beta k r_1 - c\dot{r}_2 - \beta k r_2 = P_A$ (5.16)

Eq'm of element 2, the skid $m\ddot{r}_2 + c\dot{r}_2 + k(1+\beta)r_2 c\dot{r}_1 - \beta k r_1 = P - P_A$ (5.17)

The load vector becomes: $\mathbf{P} = \begin{bmatrix} P_A \\ P - P_A \end{bmatrix}^T$

In the same way as before, Fourier transformation can be used to solve the system. This time the amplification of the skid is not interesting, but rather how big P_A must be to cancel out the different loads.

FT of eq. 5.16
$$\hat{r}_1\left[(2\pi \mathrm{i}\overline{f})^2\alpha m + (2\pi \mathrm{i}\overline{f})c + \beta k\right] - \hat{r}_2\left[(2\pi \mathrm{i}\overline{f})c + \beta k\right] = \hat{P}_A$$

Hence:
$$\hat{r}_1 = \frac{\left[(2\pi \mathrm{i}\overline{f})c + \beta k\right]\hat{r}_2 + \hat{P}_A}{-4\pi^2\overline{f}^2\alpha m + (2\pi \mathrm{i}\overline{f})c + \beta k} \tag{5.18}$$

FT of eq. 5.17
$$\hat{r}_2\left[(2\pi \mathrm{i}\overline{f})^2 m + (2\pi \mathrm{i}\overline{f})c + (1+\beta)k\right] - \hat{r}_1\left[(2\pi \mathrm{i}\overline{f})c + \beta k\right] = \hat{P} - \hat{P}_A$$

Inserting eq 5.18
$$\hat{r}_2\left[\cdots\right] = \hat{P} - \hat{P}_A\left[1 - \frac{\frac{2\pi \mathrm{i}\overline{f}c}{k} + \beta}{-B^2\alpha + \frac{2\pi \mathrm{i}\overline{f}c}{k} + \beta}\right]$$

To cancel out the load:
$$\hat{P}_A\frac{-B^2\alpha}{-B^2\alpha + \frac{2\pi \mathrm{i}\overline{f}c}{k} + \beta} = \hat{P}$$

Hence:
$$\hat{P}_A = \left[\left(1 - B^2\frac{\beta}{\alpha}\right) - \left(\frac{c}{2\pi\overline{f}\alpha m}\right)\mathrm{i}\right]\hat{P} \tag{5.19}$$

Again, if the loads are harmonic this is easily solved. The theory of these calculation is substantiated in my previous paper [14].

The amplitude of the force must be:
$$P_A = \sqrt{\left(1 - B^2\frac{\beta}{\alpha}\right)^2 + \left(\frac{c}{2\pi\overline{f}\alpha m}\right)^2}\hat{P} \tag{5.20}$$

As α approaches zero the necessary force amplitude of the actuator, P_A, approaches infinity. This is explainable because if it does not have any mass to apply pressure on, it can not generate any force on the skid, recall Newton's third law.

As α approaches infinity the necessary force amplitude of the actuator approaches $1 \cdot P$. This is also explainable because if the TMD is way greater then the skid itself, it would be like the actuator was mounted between the skid and a fixed wall. Then it would be trivial that an equal magnitude is required from the actuator to cancel out the force.

When the parameters are somewhere in between the extreme values, it highly influences the necessary force amplitude of the actuator and some advantages can be gained from equation 5.20.

The phase angle is not important because it can be manipulated with the regulation system of the actuator. The necessary amplitude of the actuator however, is important because it indicates the size of the actuator which is needed. Equation 5.20 is implemented into the MatLab function so the force needed to cancel out the different frequencies can be monitored while varying the parameters.

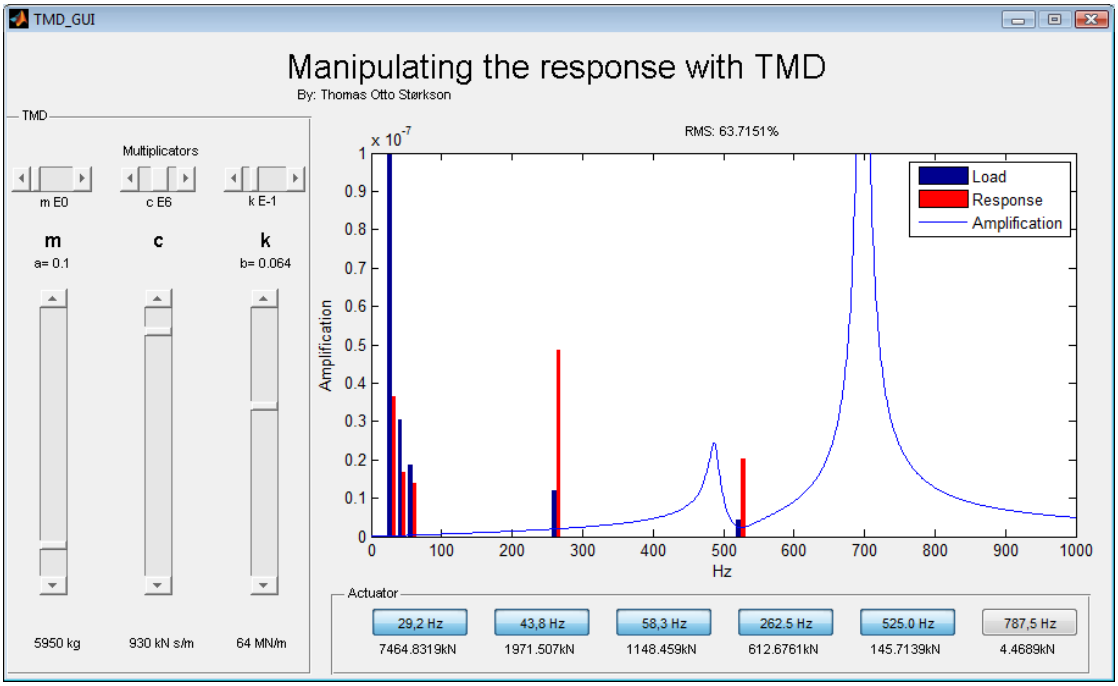

Fig. 5.27: MatLab GUI, with TMD and actuator

In the case I found most feasible, figure 5.27, an actuator with $P_A = 4489N$ at 787,5 Hz is needed. Recall that the force associated with the load at this frequency is more than 13 times higher than this. It is truly some advantages of implementing the actuator between the skid and the TMD. To get a physical interpretation of the magnitude, it is equivalent to a mass of 1,4kg rotating 0,2m off-axis. Recall that $F = mr(2\pi f)^2$ from my previous paper [14]. Therefore an actuator is an effective way to cancel out high frequency loads.

The small actuator seems to decrease the RMS vibration level with additional 6%, hence a total saving of 36% can be achieved.

As insinuated in the theory, there are also some drawbacks; additional weight is introduced to the system, and it is exposed to additional risk and maintenance work. If the system is not working exactly as predicted, resonance can develop, leading to a vastly increase of vibrations.

5.2.5 Results

Since the active dampers are based on the idea of having low mass compared to the system, they are inefficient for suppressing low frequency vibrations. An actuator is also unsuitable for cancelling out low frequency vibrations because of the required force to do so.

For the rail road tracks the main issue is airborne noise, hence it is essential to

suppress high frequency vibrations. In this case on the other hand, the main issue is structure-born noise, which implies that low frequency vibration becomes the bigger issue. I have been informed at FRAMO that reducing the mass of the FWP module is another big aim, and that increased weight of the module would result in fines. Because active damping introduces additional mass to the system, it is highly undesirable.

6. FINAL RESULTS

6.1 Inaccuracies

There are some inaccuracies regarding the equipment used to measure vibrations and the simplifications of the models used for analysis. Also the fact that I have mainly studied vibrations in y-direction generates some elements of uncertainty. The constant damping ratio applied to finite element solver also contribute to uncertainty of the quantitative results, although they do not affect the eigenfrequencies much.

Rather than focusing on the specific values achieved in this paper, one should put emphasis on the general trends.

6.2 Conclusion

A factory acceptance test is performed making sure that the equipment is within acceptance criteria regarding vibration. The equipment seems to be well within limits. Still, Frank Mohn Flatøy A/S wishes to decrease the vibrations emitted to the deck from the fire water pump module because they generate excessive structure-born noise. The data obtained from the test is used to identify weaknesses in three different ways; by looking at the total root mean square velocity at different points of the system, by studying the response spectra at different points of the system, and lastly by studying the peak mode shapes. The indications are that the excessive vibrations are caused by the hydraulic power unit which is bolted directly on the skid without damping.

Further some potential ideas of improvement are presented. Different types of dampers are suggested, concluding with that passive dampers are the best solution although active dampers should be considered in the following analysis as well. Utilizing supportive beams is also discussed with an example from a similar project. Material substitution is also proposed, with brief material index calculations. The idea of introducing additional dampers is the solution used for the analysis.

To investigate the effect of passive dampers a comprehensive finite element analysis was carried out. Firstly by making a simplified model, then estimating the load, and finally carrying out the analysis with four different cases of the hydraulic power unit's foundation stiffness. The analysis shows that although the HPU is causing over 70% of the vibration, it is only causing around 30% of the low frequency vibration (below 100Hz). AVMs are able to reduce the vibration with almost 60%, but they are not able to reduce the low frequency vibration by more than around 5%. This is because making the system softer will decrease the eigenfrequencies, thus the high frequency loads are the

ones that get damped most efficiently. If the foundation becomes too soft, the vibrations will increase and the system will get unstable, thereby causing excessive misalignment between the diesel engine and the hydraulic power unit, which again will generate even more vibrations.

To investigate the effect of active dampers a more trivial dynamic analysis was carried out with only two degrees of freedom. The load was also highly simplified, but still some conclusions can be drawn. The effect of implementing an actuator is also investigated. These techniques are most efficient for suppressing high frequency loads (by approximately 30%). This however, is something that the passive dampers do more efficiently. In addition, this solution would increase the total mass of the system which is highly undesirable.

The final conclusion is therefore that it seems to be a good idea to introduce passive dampers (anti vibration mounts) underneath the hydraulic power unit as long as the foundation does not get too soft. Even though AVMs are not able to decrease the low frequency vibrations notably, they would still decrease the total vibrations significantly. If limiting the low frequency vibrations is the main goal, this solution is not satisfactory.

6.3 Further work

- Determining the noise significant frequencies

  An interesting analysis would be to measure the noise caused by the FWP module where it is annoying for the workers. For instance, if the problem with the noise requirements are extensive noise in the control room due to FWP module vibration, the noise could be measured. Fourier transforming the noise and comparing it to the vibrations emitted to the deck, might better the understanding of which frequencies which are amplified the most through the deck.

- Study the effect of making the diesel engine foundation stiffer

  By making the DE AVMs stiffer, the eigenfrequencies are increased. This will probably result in increased vibrations, but the low frequency vibration might be reduced.

  A preposterous idea could be to mount the diesel engine directly on the skid so that the momentum of the tank and enclosure would resist the low frequency vibration of the engine. To isolate the other equipment from the skid vibrations they could be mounted on AVMs. In addition, to prevent the skid vibration to get emitted to the dect, AVMs could be placed at the module support points.

- Material substitution

  By studying a simple material index it is shown that carbon fibre composite has superior dynamic properties compared to the material that is used. The use of composite materials, in for example the engine casing, would probably reduce the magnitude of the dynamic forces greatly. In addition, material substitution would reduce the total weight of the FWP module which is another big goal.

APPENDIX

A. INTERPOL.M

```
function A=interpol(B)

%Defining new vector

n=length(B);
A=zeros(2*n,1);

%Interpolating

for i=1:2:2*n-1
        A(i)=B((i+1)/2);
        if i==2*n-1
            A(i+1)=A(i);
        else
            A(i+1)=( B((i+1)/2)+B((i+1)/2+1) )/2;
        end
end

%Deleting unmatching entries

A(end)=[];
A(end)=[];
A(end)=[];
```

B. FORCE.M

```
%Import all the spectra manually, (.txt-files)

f=PB_y(:,1);
n=length(PB_y);

%% Interpolating

PB_PB=interpol(PB_PB_import(:,2));
PB_DE=interpol(PB_DE_import(:,2));
PB_HPU=interpol(PB_HPU_import(:,2));

DE_PB=interpol(DE_PB_import(:,2));
DE_DE=interpol(DE_DE_import(:,2));
DE_HPU=interpol(DE_HPU_import(:,2));

HPU_PB=interpol(HPU_PB_import(:,2));
HPU_DE=interpol(HPU_DE_import(:,2));
HPU_HPU=interpol(HPU_HPU_import(:,2));

PB_SUP=interpol(PB_SUP_import(:,2));
DE_SUP=interpol(DE_SUP_import(:,2));
HPU_SUP=interpol(HPU_SUP_import(:,2));

%% Assembling
PB_PB_MAT=sparse(diag(PB_PB));
PB_DE_MAT=sparse(diag(PB_DE));
PB_HPU_MAT=sparse(diag(PB_HPU));

DE_PB_MAT=sparse(diag(DE_PB));
DE_DE_MAT=sparse(diag(DE_DE));
DE_HPU_MAT=sparse(diag(DE_HPU));

HPU_PB_MAT=sparse(diag(HPU_PB));
HPU_DE_MAT=sparse(diag(HPU_DE));
HPU_HPU_MAT=sparse(diag(HPU_HPU));
```

```
GIANT=[ PB_PB_MAT,  DE_PB_MAT,  HPU_PB_MAT;
        PB_DE_MAT,  DE_DE_MAT,  DE_HPU_MAT;
        PB_HPU_MAT, DE_HPU_MAT, HPU_HPU_MAT];

RESPONSE=[PB_y(:,2);DE_y(:,2);HPU_y(:,2)];

%% Solving

LOADS=GIANT\RESPONSE;

PB_load=LOADS(1:n);
DE_load=LOADS(n+1:2*n);
HPU_load=LOADS(2*n+1:end);

SUP_resp=PB_load.*PB_SUP+DE_load.*DE_SUP+HPU_load.*HPU_SUP;

%% Post processing

%Figure 1: Model verification
figure(1)
area(f,SUP_y2(:,2)/sqrt(2))
hold on
plot(f,SUP_resp/sqrt(2),':r')
xlabel('Frequency [Hz]')
ylabel('RMS velocity [m/s]')
title('Model verification')
legend('Measured response','Estimated response')
axis([2 1000 0 .9e-3])

%Figure 2: Equipment contribution
RESP_PB=PB_load.*PB_SUP;
rms_PB=sqrt(sum(RESP_PB.*RESP_PB))*1000*sqrt(1/1.5)/sqrt(2);
RESP_DE=DE_load.*DE_SUP;
rms_DE=sqrt(sum(RESP_DE.*RESP_DE))*1000*sqrt(1/1.5)/sqrt(2);
RESP_HPU=HPU_load.*HPU_SUP;
rms_HPU=sqrt(sum(RESP_HPU.*RESP_HPU))*1000*sqrt(1/1.5)/sqrt(2);
Y=[RESP_PB,RESP_DE,RESP_HPU]/sqrt(2);

figure(2)
area(f,Y)
legend('PB','DE','HPU')
axis([2 1000 0 2e-4])
```

```
title('Equipment contribution to deck vibration')
xlabel('Frequency [Hz]')
ylabel('RMS velocity [m/s]')

%Figure 3: Loads and deck response
figure(3)
subplot(3,3,1)
plot(f,PB_load)
xlabel('Frequency [Hz]')
ylabel('F_{PB} [kN]')
axis([2 1000 0 1])
subplot(3,3,2)
plot(f,DE_load)
xlabel('Frequency [Hz]')
ylabel('F_{DE} [kN]')
axis([2 1000 0 50])
subplot(3,3,3)
plot(f,HPU_load)
xlabel('Frequency [Hz]')
ylabel('F_{HPU} [kN]')
axis([2 1000 0 50])
subplot(3,3,4)
plot(f,PB_SUP)
xlabel('Frequency [Hz]')
ylabel('FRF_{PB} [m/(s kN)]')
axis([2 1000 0 1e-4])
subplot(3,3,5)
plot(f,DE_SUP)
xlabel('Frequency [Hz]')
ylabel('FRF_{DE} [m/(s kN)]')
axis([2 1000 0 1e-4])
subplot(3,3,6)
plot(f,HPU_SUP)
xlabel('Frequency [Hz]')
ylabel('FRF_{HPU} [m/(s kN)]')
axis([2 1000 0 1e-4])
subplot(3,3,7:9)
plot(f,SUP_resp/sqrt(2))
xlabel('Frequency [Hz]')
ylabel('RMS velocity [m/s]')
axis([2 1000 0 .5e-3])
```

C. PLOT_VARIABLE_K.M

```
%Change k5, k6, k7 and k8 (blanc) manually

%RMS are multiplied with Hanning windows
rms_init=sqrt(sum(SUP_resp.*SUP_resp))*1000*sqrt(1/1.5)/sqrt(2);
rms_init_low=sqrt(sum(SUP_resp(1:91).*SUP_resp(1:91)))*1000* ...
sqrt(1/1.5)/sqrt(2);

PB_SUP_v=interpol(PB_SUP_k5_import(:,2));
DE_SUP_v=interpol(DE_SUP_k5_import(:,2));
HPU_SUP_v=interpol(HPU_SUP_k5_import(:,2));

SUP_resp_v=PB_load.*PB_SUP_v+DE_load.*DE_SUP_v+HPU_load.*HPU_SUP_v;
rms_current=sqrt(sum(SUP_resp_v.*SUP_resp_v))*1000*sqrt(1/1.5)/sqrt(2);
rms_current_low=sqrt(sum(SUP_resp_v(1:91).*SUP_resp_v(1:91)))*1000...
*sqrt(1/1.5)/sqrt(2);
rms_ratio=rms_current/rms_init*100;
rms_ratio_low=rms_current_low/rms_init_low*100;

%% Plotting
figure(3)

subplot(3,3,1)
plot(f,PB_load)
xlabel('Frequency [Hz]')
ylabel('F_{PB} [kN]')
axis([2 1000 0 1])

subplot(3,3,2)
plot(f,DE_load)
xlabel('Frequency [Hz]')
ylabel('F_{DE} [kN]')
axis([2 1000 0 50])

subplot(3,3,3)
plot(f,HPU_load)
```

```
xlabel('Frequency [Hz]')
ylabel('F_{HPU} [kN]')
axis([2 1000 0 50])

subplot(3,3,4)
plot(f,PB_SUP_v)
xlabel('Frequency [Hz]')
ylabel('FRF_{PB} [m/(s kN)]')
axis([2 1000 0 1e-4])

subplot(3,3,5)
plot(f,DE_SUP_v)
xlabel('Frequency [Hz]')
ylabel('FRF_{DE} [m/(s kN)]')
axis([2 1000 0 1e-4])

subplot(3,3,6)
plot(f,HPU_SUP_v)
xlabel('Frequency [Hz]')
ylabel('FRF_{HPU} [m/(s kN)]')
axis([2 1000 0 1e-4])

subplot(3,3,7:9)
plot(f,SUP_resp_v/sqrt(2))
xlabel('Frequency [Hz]')
ylabel('RMS velocity [m/s]')
axis([2 1000 0 .5e-3])

disp(['RMS ratio [2-1000]Hz = ' num2str(rms_ratio) '%,  ...
and RMS ratio [2-100]Hz = ' num2str(rms_ratio_low) '%'])
```

D. DISPLACEMENTS.M

```
%Change k5, k6, k7 and k8 manually to get the different displacements

disp_PB_HPU_v=interpol(disp_PB_HPU_k5_import(:,2));
disp_PB_DE_v=interpol(disp_PB_DE_k5_import(:,2));

disp_DE_HPU_v=interpol(disp_DE_HPU_k5_import(:,2));
disp_DE_DE_v=interpol(disp_DE_DE_k5_import(:,2));

disp_HPU_HPU_v=interpol(disp_HPU_HPU_k5_import(:,2));
disp_HPU_DE_v=interpol(disp_HPU_DE_k5_import(:,2));

disp_HPU=PB_load.*disp_PB_HPU_v+DE_load.*disp_DE_HPU_v+HPU_load.* ...
disp_HPU_HPU_v;
disp_DE=PB_load.*disp_PB_DE_v+DE_load.*disp_DE_DE_v+HPU_load.* ...
disp_HPU_DE_v;

disp_worst=disp_HPU+disp_DE;
worst_peak=sqrt(sum(disp_worst.*disp_worst))*1000*sqrt(1/1.5)
```

E. PLOT_VARIABLE_D.M

```
%RMS are multiplied with Hanning windows
rms_init=sqrt(sum(SUP_resp.*SUP_resp))*1000*sqrt(1/1.5)/sqrt(2);
rms_init_low=sqrt(sum(SUP_resp(1:91).*SUP_resp(1:91)))*1000* ...
sqrt(1/1.5)/sqrt(2);

PB_SUP=interpol(PB_SUP_import(:,2));
DE_SUP=interpol(DE_SUP_import(:,2));
HPU_SUP=interpol(HPU_SUP_import(:,2));

PB_SUP_d2=interpol(PB_SUP_d2_import);
DE_SUP_d2=interpol(DE_SUP_d2_import);
HPU_SUP_d2=interpol(HPU_SUP_d2_import);

PB_SUP_d6=interpol(PB_SUP_d6_import);
DE_SUP_d6=interpol(DE_SUP_d6_import);
HPU_SUP_d6=interpol(HPU_SUP_d6_import);

RSUP=PB_load.*PB_SUP+DE_load.*DE_SUP+HPU_load.*HPU_SUP;
RSUP_d2=PB_load.*PB_SUP_d2+DE_load.*DE_SUP_d2+HPU_load.*HPU_SUP_d2;
RSUP_d6=PB_load.*PB_SUP_d6+DE_load.*DE_SUP_d6+HPU_load.*HPU_SUP_d6;

rms_current=sqrt(sum(RSUP.*RSUP))*1000*sqrt(1/1.5)/sqrt(2);
rms_current_low=sqrt(sum(RSUP(1:91).*RSUP(1:91)))*1000* ...
sqrt(1/1.5)/sqrt(2);
rms_ratio=rms_current/rms_init*100;
rms_ratio_low=rms_current_low/rms_init_low*100;

rms_current_d2=sqrt(sum(RSUP_d2.*RSUP_d2))*1000*sqrt(1/1.5)/sqrt(2);
rms_current_low_d2=sqrt(sum(RSUP_d2(1:91).*RSUP_d2(1:91)))*1000* ...
sqrt(1/1.5)/sqrt(2);
rms_ratio_d2=rms_current_d2/rms_init*100;
rms_ratio_low_d2=rms_current_low_d2/rms_init_low*100;

rms_current_d6=sqrt(sum(RSUP_d6.*RSUP_d6))*1000*sqrt(1/1.5)/sqrt(2);
rms_current_low_d6=sqrt(sum(RSUP_d6(1:91).*RSUP_d6(1:91)))*1000* ...
```

```
sqrt(1/1.5)/sqrt(2);
rms_ratio_d6=rms_current_d6/rms_init*100;
rms_ratio_low_d6=rms_current_low_d6/rms_init_low*100;

%% Plotting
figure(1)

subplot(3,3,1)
plot(f,PB_load)
xlabel('Frequency [Hz]')
ylabel('F_{PB} [kN]')
axis([2 1000 0 1])

subplot(3,3,2)
plot(f,DE_load)
xlabel('Frequency [Hz]')
ylabel('F_{DE} [kN]')
axis([2 1000 0 50])

subplot(3,3,3)
plot(f,HPU_load)
xlabel('Frequency [Hz]')
ylabel('F_{HPU} [kN]')
axis([2 1000 0 50])

subplot(3,3,4)
plot(f,PB_SUP_d2,'r',f,PB_SUP,'b',f,PB_SUP_d6,'g')
legend('CDR = 2%','CDR = 4% (default)','CDR = 6%')
xlabel('Frequency [Hz]')
ylabel('FRF_{PB} [m/(s kN)]')
axis([2 1000 0 1e-4])

subplot(3,3,5)
plot(f,DE_SUP_d2,'r',f,DE_SUP,'b',f,DE_SUP_d6,'g')
legend('CDR = 2%','CDR = 4% (default)','CDR = 6%')
xlabel('Frequency [Hz]')
ylabel('FRF_{DE} [m/(s kN)]')
axis([2 1000 0 1e-4])

subplot(3,3,6)
plot(f,HPU_SUP_d2,'r',f,HPU_SUP,'b',f,HPU_SUP_d6,'g')
legend('CDR = 2%','CDR = 4% (default)','CDR = 6%')
xlabel('Frequency [Hz]')
```

```
ylabel('FRF_{HPU} [m/(s kN)]')
axis([2 1000 0 1e-4])

subplot(3,3,7:9)
plot(f,RSUP_d2,'r',f,RSUP,'b',f,RSUP_d6,'g')
legend('CDR = 2%','CDR = 4% (default)','CDR = 6%')
xlabel('Frequency [Hz]')
ylabel('RMS velocity [m/s]')
axis([2 1000 0 .5e-3])

disp(['CDR=2% : RMS ratio [2-1000]Hz = ' num2str(rms_ratio_d2) '%, ...
        and RMS ratio [2-100]Hz = ' num2str(rms_ratio_low_d2) '%'])

disp(['CDR=4% : RMS ratio [2-1000]Hz = ' num2str(rms_ratio) '%, ...
   and RMS ratio [2-100]Hz = ' num2str(rms_ratio_low) '%'])

disp(['CDR=6% : RMS ratio [2-1000]Hz = ' num2str(rms_ratio_d6) '%, ...
and RMS ratio [2-100]Hz = ' num2str(rms_ratio_low_d6) '%'])
```

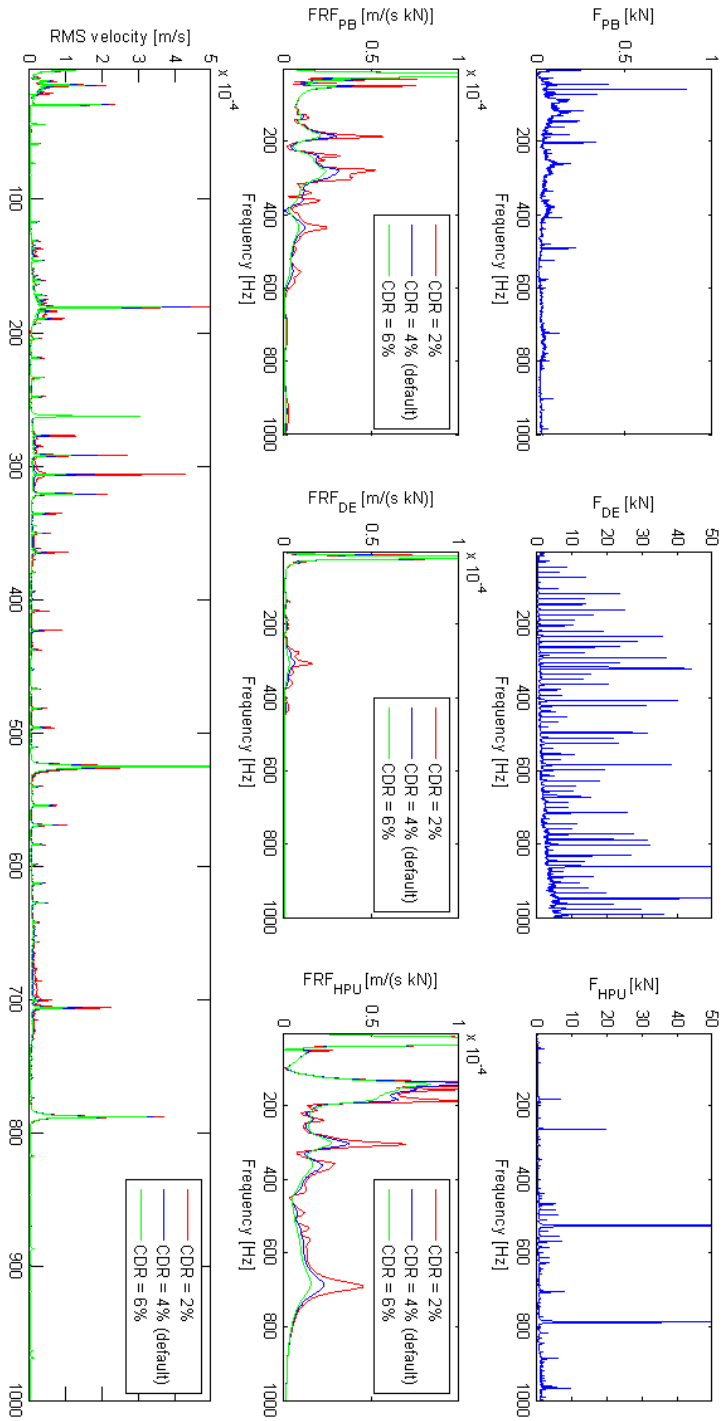

Fig. E.1: The effect of constant damping ratio

F. SPEC2.M

```
function [f X Y Y2 H A]=spec2(a,b,c)

%Initializing
n=1000;
f=linspace(1,1000,n);
H=zeros(1,n);

%Defining constants
m=5.95E4; %kg
k=1E12; %N/m

%Simulating transfer function
for i=1:n
    w=f(i)*2*pi;
    H(i)=abs(w*(-w^2*m+1i*w*c+k*(1+b)-(1i*w*c+b*k)^2/(-w^2*a*m+1i*w*c+b*k))^-1);
    B2=4*pi^2*f(i)^2*m/k;
    H(i)=abs(2*pi*f(i)/(k*( 1-B2*(1+a)-(a*B2)^2/(b+2*pi*f(i)*c*1i/k-a*B2) )));
    Act(i)=abs(1-(2*pi*1i*f(i)*c/k+b)/(B2*a));
    Act(i)=abs(  (1-B2*b/a)-(c/(2*pi*f(i)*a*m))*1i  );
end


%f1=f(293)
%f2=f(438)
%f3=f(583)
%f4=f(2626)
%f5=f(5251)
%f6=f(7875)
X=[29.17 43.75 58.33 262.5 525 787.5];
Y=[5.67E6 1.72E6 1.06E6 6.80E5 2.48E5 6.07E4];
Y2=[H(29),H(44),H(58),H(263),H(525),H(788)].*Y;
A=[Act(29),Act(44),Act(58),Act(263),Act(525),Act(788)].*Y;
```

G. ELECTRONIC APPENDIX

A lot of the desired appendix are unsuitable to attach on paper. The following are included in the attached file: **ElectronicAttachments.zip**

- The visualization of the mode shapes described in section 4.1.3.

  ElectronicAttachments\Mode Shape Animations\

- The moment of inertia calculations from section 5.1.

  ElectronicAttachments\Spreadsheets\

- All the above MatLab scripts (except spec2.m) in addition to the FRFs generated with Ansys, used in section 5.1.

  ElectronicAttachments\MatLab\AMD\

- The MatLab GUI and spec2.m used in section 5.2.

  ElectronicAttachments\MatLab\TMD\

BIBLIOGRAPHY

[1] http://matweb.com/.

[2] Frank Mohn Flatøy A/S. Vibration Acceptance Criteria for Diesel Hydraulic and Submerged Hydraulic Driven Pump.

[3] M.F. Ashby. Material Selection in Mechanical Design, 2nd edn, Chapter 6. Butterworth-Heinemann, Oxford, 1999.

[4] M.F. Ashby and D. Cebon. Case Studies in Material Selection. Granta Design, Trumpington, 1995.

[5] Centa. CentaFlex-A.

[6] Anil K. Chopra. Dynamics of Structures. Pearson, 2007.

[7] Hari Dharan. Mechanical Behaviour of Composite Materials. UC Berkeley, 2010.

[8] Framo. Harmonic response analysis and vibration measurment Pazflor FPSO FWP. Technical report, Pazflor, 2009.

[9] M.J. Griffin. Handbook of human vibrations. Academic Press Ltd, 1990.

[10] Brüel & Kjær. Modal Analysis Course Booklet, 2001.

[11] Bomel Ltd. Noise and Vibration. Technical report, HSE, 2001.

[12] RubberDesign. Conical Mountings.

[13] Springer. Noise and Vibration Mitigation for Rail Transportation Systems, 2012.

[14] Thomas Otto Størkson. Theory of Fire Water Pump Dynamics. 2011.

[15] Einar N. Strømmen. Theory of Bridge Aerodynamics. Springer, 2010.

[16] Charles Fayette Taylor. Internal Combustion Engine in Theory and Practice. MIT Press, 1985.

[17] VibraTec. Vibration Control in Oil and Gas Industry, 2011.

[18] Banting Wong Wilson Ho and David England. Tuned Mass Damper for Rail Noise Control. Technical report, MTR Corporation, 2012.